

# Testing cold dark matter with the low mass Tully-Fisher relation

Michael R. Blanton<sup>1</sup>, Marla Geha<sup>2</sup>, and Andrew A. West<sup>3</sup>

## ABSTRACT

In most cosmological theories, the galaxy mass function at small masses is related to the matter power spectrum on small scales. The circular velocity function (a quantity closely related to the mass function) is well-studied for dwarf satellites in the Local Group. However, theoretical predictions and observational measurements are difficult for satellite galaxies, because of ram pressure and tidal stripping. By contrast, isolated dwarf galaxies are less affected by these processes, and almost always have enough 21cm emission to trace their dynamics robustly. Here, we use isolated low mass dwarf galaxies from the Sloan Digital Sky Survey (SDSS), with measured 21cm widths, to test cold dark matter cosmology. We find consistency between the predicted and observed number density of isolated galaxies down to  $V_{\max} \sim 50 \text{ km s}^{-1}$ . Our technique yields a direct test of small-scale cosmology independent of the Lyman- $\alpha$  forest power spectrum, but our sample is currently statistically less powerful: warm dark matter particles heavier than 0.5 keV cannot be ruled out. Our major systematic uncertainty is the surface brightness limit of the SDSS. Blind HI surveys, such as the ALFALFA survey on Arecibo, are expected to uncover a much larger number of isolated low mass galaxies, will increase the power of our constraints at small scales, and will propel the study of isolated galaxies to low masses previously attainable only in the Local Group. We use our sample to explore dwarf galaxy formation as well, finding that the Tully-Fisher relation for dwarf galaxies is a strong function of environment, and that the baryon (stellar plus neutral gas mass) fraction is only a weak function of galaxy mass. Together with the strong dependence of gas fraction on environment, these results indicate that for dwarf galaxies, gas loss and the end of star-formation are dominated by external, not internal, processes.

*Subject headings:* galaxies: dwarf — galaxies: kinematics and dynamics — cosmology: observations

## 1. Introduction: the mass function and cosmology

A critical test for any theory of cosmology and structure formation is whether it correctly predicts the galaxy mass function. The current Cold Dark Matter model with a cosmological constant ( $\Lambda$ CDM; Spergel et al. 2006) makes robust predictions for the number of dark matter halos as a function of mass, finding roughly that  $dN/dM \propto M^{-1.8}$  (Sheth et al. 2001; Jenkins et al. 2001; Reed et al. 2003; Yahagi et al. 2004). A similar mass function describes the distribution of surviving subclumps within the dark matter halos (“subhalos”) that most investigators associate with the sites of galaxy formation (Colín et al. 1999;

<sup>1</sup> Center for Cosmology and Particle Physics, Department of Physics, New York University, 4 Washington Place, New York, NY 10003

<sup>2</sup> National Research Council of Canada, Herzberg Institute of Astrophysics, 5071 West Saanich Road, Victoria, BC V9E 2E7, Canada

<sup>3</sup> Astronomy Department, University of California, 601 Campbell Hall, Berkeley, CA 94720

Gao et al. 2004; Kravtsov et al. 2004a; Reed et al. 2005; Zentner et al. 2005; Conroy et al. 2005). Of course, extending this model to predict the number density of galaxies in the Universe requires including physical effects such as gas cooling, star-formation, supernova feedback, and possibly the formation of supermassive black holes and their feedback, that are too complex to follow exactly in numerical predictions. Nevertheless, in the last three decades numerous approximate approaches to the problem have lent us some understanding of what the correct predictions might be and what physical processes a successful model may involve (e.g., Rees & Ostriker 1977; White & Rees 1978; White & Frenk 1991; Blanton et al. 1999; Somerville et al. 2001; Benson et al. 2003; Robertson et al. 2005; Croton et al. 2006).

Recently, various investigators have tested the halo mass function at high masses and found consistency with predictions based on Wilkinson Microwave Anisotropy Probe three-year (WMAP3) cosmological parameters (Bahcall et al. 2003; Rines et al. 2006; Eke et al. 2006). In addition, for individual, high luminosity galaxies one can perform a similar test. If galaxy luminosity is related monotonically (with some scatter) to halo mass, then  $\Lambda$ CDM predicts the weak-lensing signal as a function of galaxy abundance. Tasitsiomi et al. (2004) have verified this prediction for galaxies with  $L_r > L_{r,*}$ , and Seljak et al. (2005) have performed a similar test extending down to about  $0.1L_{r,*}$ .

Below  $0.1L_{r,*}$ , the luminosity function is closer to a power law, with a slope that varies somewhat over luminosity but is never steeper than about  $N \propto L^{-1.5}$  at most, significantly shallower than the prediction for the number as a function of halo mass (Trentham et al. 2005; Blanton et al. 2005). If galaxies and subhalos are associated one-to-one, then the mass-to-light ratios of galaxies must increase substantially with decreasing luminosity. However, data on galaxies at the lowest luminosities has in the past been rather scarce. At circular velocities below  $L_r \sim 0.1L_{r,*}$  nobody has demonstrated consistency between the  $\Lambda$ CDM prediction and the galaxy mass function. Some valiant attempts exist, but rely on extrapolating the Tully & Fisher (1977) and Faber & Jackson (1976) relations into the low luminosity regime (Desai et al. 2004; Goldberg et al. 2005).

The most extreme example of this issue is the “substructure problem” in the Local Group (Klypin et al. 1999; Kravtsov et al. 2004b).  $\Lambda$ CDM predicts hundreds of low mass satellites of the Milky Way, but only approximately twenty are known (though the number is growing month by month; Ibata et al. 1995; Mateo 1998; Willman et al. 2005a,b; Belokurov et al. 2006; Zucker et al. 2006a,b). Simon & Geha (2007) show that although the newly discovered galaxies have eased this discrepancy, a factor of 2–4 difference remains even when reasonable baryonic physics has been taken into account. This test of cosmology probes the lowest mass galaxies possible, and so is extremely sensitive to differences in the mass function slope. However, both predictions and observations are quite difficult in the vicinity of a luminous galaxy. From the point of view of theory, a number of processes, such as tidal stripping, ram pressure stripping, dynamical friction, and merging onto the large galaxy, can occur near luminous galaxies (Kravtsov et al. 2004b; Bullock & Johnston 2005; Zentner et al. 2005; Mayer et al. 2006). When a dwarf galaxy enters the environment of a large galaxy, tidal stripping can reduce its mass. In addition, the larger dwarf galaxies are preferentially dragged to the center and merge with the large galaxy. All of these processes alter the predicted mass function, but to follow them all requires difficult-to-execute and physically uncertain simulations. From the point of view of observations, the ram pressure stripping removes any existing neutral gas disks, the component of dwarf galaxies known to extend furthest out into the dark matter halo (Stoehr et al. 2002). With only the stars, it is difficult to probe any dark halo that might still surround a Local Group dwarf.

On the other hand, isolated dwarf galaxies are possibly much simpler systems. Without a large galaxy nearby, the physical processes described in the previous paragraph cannot occur, simplifying the prediction of their mass function. In addition, as it happens, isolated dwarf galaxies essentially always have intact HI disks (Geha et al. 2006a), allowing us to probe their masses out to large radii with relative ease (Swaters et al.

2002). The disadvantage of isolated dwarf galaxies is that they are far away, making them difficult to find at the lowest luminosities.

This paper represents a first step at examining the low mass end of the mass function for isolated galaxies. We use a sample of dwarf galaxies selected from the Sloan Digital Sky Survey (SDSS; York et al. 2000). From the SDSS, we evaluate their number densities, and we estimate their maximum circular velocity using single-beam HI profiles taken using the Arecibo Observatory and the Green Bank Telescope. We compare these observations to theoretical predictions for the number density of isolated halos of the same circular velocity. By comparing circular velocities, we avoid the considerable theoretical and observational uncertainties in determining the total mass of halos and galaxies. While this approach represents a beginning, we discuss in the conclusions how we can improve our observational estimates of the masses and number densities of these objects, and also find lower mass galaxies. With a much larger sample of isolated low mass galaxies, our technique can provide a stringent and unique constraint on the power spectrum at small scales.

In Section 2, we describe the optical and radio observations our results are based on. In Section 3, we describe the Tully-Fisher relationship for isolated galaxies. In Section 4, we describe our theoretical models. In Section 5, we compare the observations to the theory. In Section 6, we explore the robustness of our results to our definition of “isolation” in this context. In Section 7, we examine the relationships among the baryonic, stellar, and total mass estimates in our sample. In Section 8, we describe how these results might be improved upon in the future. Finally, in Section 9, we summarize our results.

For determining luminosity distances and other derived parameters from observations, we have assumed cosmological parameters  $\Omega_0 = 0.3$ ,  $\Omega_\Lambda = 0.7$ , and  $H_0 = 100 h \text{ km s}^{-1} \text{ Mpc}^{-1}$ . Where necessary, we have used  $h = 0.7$ ; otherwise, we have left the dependence on  $h$  explicit. All magnitudes in this paper are  $K$ -corrected to rest-frame bandpasses using the method of Blanton et al. (2003) and `kcorrect v4_1_4`, unless otherwise specified. Because of the small range of look-back times in our sample (a maximum of around 700 Myr), we do not evolution-correct any of our magnitudes.

## 2. Observations

### 2.1. Sloan Digital Sky Survey

To evaluate the luminosity function of dwarf galaxies, we use a modified version of the SDSS spectroscopic catalog. Blanton et al. (2005) describe our sample, which is a subsample of the New York University Value-Added Galaxy Catalog (NYU-VAGC; Blanton et al. 2005). We have updated that catalog from SDSS Data Release 2 to Data Release 4 (DR4; Adelman-McCarthy et al. 2006). The Blanton et al. (2005) catalog represents a significant improvement over naïvely selecting galaxies from the SDSS catalog, which is not optimized for nearby, low surface brightness galaxies. It is selected with an optical flux limit of  $m_r \sim 17.8$ . For each galaxy, the catalog provides the SDSS redshift, emission line measurements, multi-band photometry, structural measurements and environment estimates (for more catalog details see Blanton et al. 2005). Distances are estimated based on a model of the local velocity field (Willick et al. 1997). Distance errors have been folded into error estimates of all distance-dependent quantities such as absolute magnitude and HI mass.

For our purposes, this catalog suffers from one major selection effect, due to the difficulty of detecting low surface brightness galaxies in the optical. As shown in Blanton et al. (2005), the completeness as a function of half-light surface brightness drops below 50% at  $\mu_{50,r} \sim 23.5 \text{ mag arcsec}^{-2}$ . Blanton et al. (2005) present

a simple model for the effect that surface brightness has on the completeness, which assumes a log-normal surface brightness distribution with a mean that decreases as luminosity decreases. Figure 1 shows what this model implies about the missing fraction of galaxies as a function of luminosity in our sample, in terms of the correction factor  $c$  we must apply to recover the “correct” number density at each luminosity. For comparison, we also show the equivalent factor for dwarf galaxies in the Local Group (Mateo 1998) given the SDSS surface brightness cutoff, and in the local catalog of Karachentsev et al. (2004). Note that the Karachentsev et al. (2004) curve is complicated by the fact that the quantities in the catalog (Holmberg radius and flux) are not enough to infer a half-light surface brightness (the terms in which we have calculated the completeness) uniquely in general, even if we assume an exponential profile. The Mateo (1998) and Karachentsev et al. (2004) catalogs bracket our correction factor of 1.7 at  $M_r - 5 \log_{10} h \sim 15$ , indicating it is roughly correct to within 20%. Therefore, we use the model of Blanton et al. (2005) to correct the luminosity functions we present here — without any *a posteriori* corrections. Nevertheless, the uncertainty of how many galaxies we are missing due to this effect is the most worrying one affecting our results.

## 2.2. Environments of galaxies

As argued above, there are advantages to finding *isolated* galaxies with which to test the circular velocity and mass functions. We cannot rely on the SDSS alone to determine whether a galaxy is isolated, for several reasons. First, the angular distances between nearest neighbor galaxies can be large for this nearby sample—for example, searching a 1 Mpc region around a galaxy 30 Mpc away corresponds to 2 degrees on the sky. Many of our dwarf galaxies are on the SDSS Southern stripes, which are only 2.5 degrees wide. In addition, because the SDSS reduction software is not optimized for large, extended objects and fails to process them correctly, the SDSS catalog does not contain many of the bright galaxies within 30 Mpc. Thus, to calculate the environments of our dwarf galaxy sample, we need a supplemental catalog that extends beyond the SDSS area and contains the brightest galaxies.

Both of these considerations drive us to use the The Third Reference Catalog of Galaxies (RC3; de Vaucouleurs et al. 1991), which is a nearly complete catalog of nearby galaxies. To determine environments for our dwarf galaxies, we must determine the distance of each to its nearest “luminous” neighbor. In this context, we define galaxies as luminous when  $M_r - 5 \log_{10} h < -19$ , corresponding to circular velocities of  $V_c > 140 \text{ km s}^{-1}$  for galaxies on the Tully-Fisher relationship (see Section 3). From the  $B$  and  $V$  photometry listed in RC3, we infer  $M_r$  for each galaxy. For galaxies which have the relevant entries listed, we call galaxies luminous if  $M_r - 5 \log_{10} h < -19$ . For galaxies which do not have the relevant entries, but do have HI data listed, we call them luminous if  $W_{20} > 300 \text{ km s}^{-1}$  (as described in § 2.3,  $W_{20}$  is twice the maximum circular velocity of the HI gas). Finally, there are some galaxies with neither HI data nor optical photometry listed in RC3. For this small set, we extract the “magnitude” from NED (which empirically is very similar to the  $B$  band RC3 magnitude for galaxies which have both) and guess  $M_r$  based on that magnitude. We call these galaxies luminous if  $M_r - 5 \log_{10} h < -19$ . Additionally, we update the coordinates in RC3 using the NASA Extragalactic Database (NED) coordinates for each of the catalog objects. This set of bright galaxies is not perfectly uniform, but is suitable for our purposes.

We combine the SDSS galaxies with  $M_r - 5 \log_{10} h < -19$  with the RC3 luminous galaxy catalog (removing repeats between the two). Then, we determine the nearest neighbor distance by asking whether there is a luminous RC3 or SDSS neighbor within  $2 h^{-1} \text{ Mpc}$  and  $400 \text{ km s}^{-1}$  in redshift for each galaxy in our sample. In this paper, we will generally refer to isolated galaxies as those with no such neighbor within  $r_{\text{lim}} = 1.0 h^{-1} \text{ Mpc}$ . However, in order to test the robustness of our results, we will vary our procedure

below by using alternate limits of  $M_r - 5 \log_{10} h < -18$  (a “fainter tracer sample”) and  $M_r - 5 \log_{10} h < -20$  (a “brighter tracer sample”). We will also vary the  $r_P$  limit, as we describe explicitly below.

We can calculate the number density of galaxies by weighting with the  $1/V_{\max}$  values that Blanton et al. (2005) describes. Of course, some of the volume actually is not available (e.g. in a cluster a galaxy will never appear isolated) and in principle we might need to account for this fact. To do so, we can measure the “isolated fraction,” the fraction of the volume of our sample which is isolated from luminous galaxies, by randomly placing points within the volume and testing their environment. This fraction is 0.95, and varies by less than 0.05 when we vary our definition of “isolated” as noted above, minor compared to our other uncertainties. Thus, we simply ignore this correction, and calculate the number density of isolated galaxies over the entire volume.

The thick line Figure 2 shows the cumulative number density of such isolated galaxies as a function of absolute magnitude, corrected for surface brightness incompleteness. This statistic depends on the definition of “isolated” that we use; the two thin lines use the fainter and brighter tracer samples described above. As this comparison shows, a change in magnitude of the tracer by about 1 mag is equivalent to a 20% change in the cumulative number density at  $M_r - 5 \log_{10} h \sim -15$ .

Taken together these data show that the number density of isolated galaxies with  $M_r - 5 \log_{10} h < -14.7$  is  $(6.83 \pm 2.3) \times 10^{-2} h^3 \text{ Mpc}^{-3}$ , with the uncertainty dominated by the definition of “isolated” and the fraction of galaxies missing due to surface brightness effects.

### 2.3. Radio observations at 21cm

Geha et al. (2006a) present the radio observations of dwarf galaxies selected from the SDSS sample described above. The data were obtained on the Green Bank 100-m Telescope (GBT) and at Arecibo Observatory. Each observation had a velocity resolution better than about  $3 \text{ km s}^{-1}$ . The optical half-light radii of the dwarf galaxies in our sample are typically  $\sim 8''$ , and should be completely contained with the radio beamsize of  $3'$  and  $9'$  for Arecibo and GBT, respectively. Here we will restrict ourselves to galaxies with detected HI (which Geha et al. 2006a showed dominated the isolated galaxy population) and with  $b/a < 0.5$  to minimize inclination effects.

We compute the 20% HI line-width (W20) by finding the peak HI flux within  $150 \text{ km s}^{-1}$  of the optical radial velocity of each galaxy and computing the difference between the nearest points having 20% of the peak flux. The integrated HI flux is calculated by expanding the W20 values by  $20 \text{ km s}^{-1}$  on each side and integrating the flux in this region. Errors bars on the line widths and integrated fluxes were computed using a Monte Carlo bootstrap method: noise was added to the stacked one-dimensional radio spectra (based on the observed variance in the baseline) and the observed quantities remeasured. We calculated error bars on the line-width and integrated flux from the scatter in the mean quantities recovered from Monte Carlo simulations.

As Geha et al. (2006a) showed, the dwarf galaxies in our sample have a significant rotation component. We derive the maximum rotation speeds as follows. We correct the observed HI line-widths for line broadening due to turbulent velocity dispersion and inclination using the formula first proposed by Bottinelli et al. (1983):

$$V_{\max} = \frac{W20 - W20_t}{\sin i}, \quad (1)$$

where  $W20$  is the observed HI line-width,  $W20_t$  is the turbulent velocity correction term and  $i$  is the

inclination angle inferred from the optical images. We confirm the validity of a linear turbulence correction by modeling the integrated velocity profiles of simulated galaxies constructed from Hernquist (1993) model disk galaxies. For nearby dwarf galaxies with rotation velocities similar to our sample, Begum et al. (2006) have measured a velocity dispersion in the gas component of  $\sigma_{\text{los}} = 8 \text{ km s}^{-1}$  from 2D velocity maps. Using the Begum et al. value, this results in a turbulence correction of  $W20_t = 16 \text{ km s}^{-1}$ , which we use here. Altering this turbulence correction (say to  $25 \text{ km s}^{-1}$ ) does not change our results below.

Figure 3 shows our best estimate of  $V_{\text{max}}$  for our dwarf galaxies (with  $b/a < 0.5$ ) as a function of the distance to the nearest luminous galaxy. Clearly there is a strong relationship between  $V_{\text{max}}$  and projected separation. Within  $1 h^{-1} \text{ Mpc}$  of luminous galaxies there is a population of objects with  $V_{\text{max}} < 40 \text{ km s}^{-1}$ , that is much rarer at large separations. Our galaxies are selected to be distributed roughly evenly in the range  $-13.5 > M_r - 5 \log_{10} h > -15.5$ , independent of environment. Thus, at these luminosities the “forward” Tully-Fisher relationship — the circular velocity at a fixed luminosity — appears to be a strong function of nearest neighbor distance. This result does not imply that no low circular velocity galaxies exist in the field, simply that any such galaxies are too low luminosity to make it into our sample.

As Geha et al. (2006a) and others have found, dwarf galaxies near a luminous neighbor also tend to be red and gas poor. Taken all together, these results suggest that some important physical effects are shaping the gas content, star-formation histories and inferred dynamics of dwarf satellite galaxies relative to isolated dwarfs. For this reason, we choose to concentrate our attention here on the isolated galaxies, whose  $V_{\text{max}}$  values have a smaller dispersion, and whose properties in general we expect to be less altered since formation, relative to those dwarfs perturbed by a massive neighbor.

Although it is immaterial to our analysis below, it is interesting to ask what physical effects are causing the trend in Figure 3. We can think of three explanations. First, for dwarfs in the vicinity of luminous galaxies, ram pressure stripping could remove gas at the largest galactocentric radii first, reducing the maximum circular velocity traced by HI emission. Second, tidal stripping could reduce the total mass and thus the circular velocities. Third, interaction-triggered star-formation could either raise the luminosities of satellite galaxies relative to isolated galaxies, bringing lower mass systems into our sample if they are near bright galaxies, or speed up star-formation and use up the gas in the outer disk of the galaxy. To help investigate this question, in Figure 3 we have distinguished between single-peaked HI profiles (open circles) and double-peaked or flat-topped profiles (filled circles), as classified by Geha et al. 2006a). Because the dwarfs with low  $V_{\text{max}}$  are predominantly single-peaked profiles (and we have enough resolution to see double-peaked profiles if they existed), we favor the explanation that gas has been stripped from the outsides. However, a definitive conclusion awaits a comprehensive analysis, including more detailed dynamics of these galaxies.

### 3. Tully-Fisher relation for isolated galaxies

Here we give an estimate of the Tully-Fisher relationship for isolated galaxies. We base our estimate on the sample described in the previous section for low luminosities, plus the recently published samples of Pizagno et al. (2006) and Springob et al. (2005) for higher luminosities.

Pizagno et al. (2006) presented a Tully-Fisher survey of galaxies found in the SDSS, using follow-up H $\alpha$  rotation curves. They have performed model fits to the disk components of these galaxies to inclination-correct their maximum circular velocities. Unlike previous Tully-Fisher samples (e.g., Courteau 1997), which were selected to be very homogeneous sets of galaxies, the Pizagno et al. (2006) sample spans a large range

of galaxy types and colors, resulting in a somewhat larger scatter in the Tully-Fisher relationship than found in other studies. For each of their galaxies we have determined its environment in the same manner as for our low luminosity sample, and we only consider isolated galaxies here. However, as Pizagno et al. (2006) show, and we have confirmed using our own measurements of environment, there is very little dependence of the Tully-Fisher relation on environment at high luminosities. As with the low luminosity sample, we restrict ourselves to galaxies with  $b/a < 0.5$ , leaving 35 galaxies from Pizagno et al. (2006).

Springob et al. (2005) have compiled HI spectra from archival data sets for around 9000 galaxies in the local Universe, observed originally with Arecibo, the 91m and 42m Green Bank telescopes, the Nançay telescope, and the Effelsberg 100m telescope. They have homogeneously analyzed these spectra, measuring their widths and HI fluxes. All their galaxies have optical data associated with them, including a measure of their axis ratio ( $b/a$ ). We use the turbulence and inclination corrections of Equation (1) to convert the  $W_{20}$  values to  $V_{\max}$ . In addition, in order to get luminosities and environments for these galaxies, we match this list to the full low-redshift catalog from SDSS DR4 (just as for our dwarf sample). Finally, we restrict this sample to the isolated galaxies with  $b/a < 0.5$ , leaving 85 galaxies from Springob et al. (2005).

Figure 4 shows the Tully-Fisher relationship for all three samples of galaxies. The low luminosity points are from our isolated sample. The crosses in Figure 4 show the median  $V_{\max}$  values in several bins centered on  $M_r - 5 \log_{10} h = -14.7, -18.5, -19.5$ , and  $-20.5$ , and 1 magnitude in width. Table 1 lists the median velocity in each bin (and several other bins needed below).

#### 4. Theory

In order to find an appropriate theoretical comparison, we use the  $N$ -body, pure dark matter simulations of Kravtsov et al. (2004a). They simulated a cubic box  $80 h^{-1}$  Mpc on a side, with  $512^3$  particles, each around  $3.2 \times 10^8 h^{-1} M_\odot$  in mass. The world model and transfer function for the simulation correspond to  $\Omega_m = 0.24$ ,  $\Omega_\Lambda = 0.76$ ,  $\Omega_b = 0$ ,  $h = 0.73$ ,  $n = 0.95$ , and  $\sigma_8 = 0.75$ . Although this cosmology is not *precisely* the current best-fit model, we describe below how we implement small corrections to account for this fact. We used the outputs from  $z = 0$ .

Dark matter halos were identified using the method described in Kravtsov et al. (2004a). They calculated the maximum circular velocity of each halo by determining the enclosed mass  $M(< R)$  as a function of radius, using the spherically symmetric approximation  $v = \sqrt{GM(< R)/R}$ , and determining the peak in the rotation curve. Strictly speaking, this  $V_{\max}$  value is only comparable to our observed galaxies if their 21cm emission probes this peak. However, because most of our galaxies show flat-topped or double-peaked HI profiles, we are probably close to satisfying this condition.

To define “isolated” we use tracer halos with  $V_{\max}$  values corresponding to the Tully-Fisher results listed in Table 1. We project the distribution of halos in a random direction, and perturb the “redshift-space” positions of the halos to account for their peculiar velocities. Then we define “isolated” in the simulation using the same geometrical considerations used in the observations ( $|\Delta v| < 400 \text{ km s}^{-1}$  and  $r_p < 1 h^{-1}$  Mpc) but relative to the tracer halo population. The velocity function of these isolated halos is shown in Figure 5 as the histograms. Down to  $70 \text{ km s}^{-1}$  each histogram comes from the simulation, but below that we extrapolate the velocity function as a power law (roughly  $\Phi(> V_{\max}) \propto V_{\max}^{-2.7}$ ). The three histograms, as labeled, correspond to tracers with  $V_{\max} > 110 \text{ km s}^{-1}$  (corresponding to galaxies with  $M_r - 5 \log_{10} h < -18$ ),  $V_{\max} > 140 \text{ km s}^{-1}$  (corresponding to galaxies with  $M_r - 5 \log_{10} h < -19$ ), and  $V_{\max} > 180 \text{ km s}^{-1}$  (corresponding to galaxies with  $M_r - 5 \log_{10} h < -20$ ). For the bulk of this paper,

we will be concerned with the central class, shown as the thick histogram, but will use the other results to quantify how much our results depend on the choice of tracer population.

Because of the complex geometrical definition of “isolated,” it is useful to have this  $N$ -body estimate of the mass function. However, the cosmology used for the simulation does not correspond precisely to the current best fit cosmology (e.g. Tegmark et al. 2006); in particular it does not include the effects of baryons on the initial power spectrum. We adjust for this difference by using the excursion set formalism and the transfer functions of Eisenstein & Hu (1998), along with the mass function approximation from Warren et al. (2006). These methods are able to predict the mass function for any hierarchical cosmology, as a function of redshift and of large-scale environment. We use a particular implementation provided by Andreas Berlind (private communication). These methods yield the mass function of galaxies, which we convert into a circular velocity function using the methods of Bullock et al. (2001b), using  $M_* = 1.5 \times 10^{12} h^{-1} M_\odot$  and  $\Omega_m = 0.24$ .

First, we need to evaluate what large-scale environment our definition of “isolated” corresponds to. The smooth line in Figure 5 is the prediction for the mass function of halos in large-scale underdensities of  $\delta = -0.4$ , for the cosmology used in Kravtsov et al. (2004a). From this agreement, we conclude that in the excursion set mass functions,  $\delta = -0.4$  is the underdensity that is most comparable to our isolation criterion.

Second, in order to adjust the results of Kravtsov et al. (2004a) for cosmology, we evaluate the ratio  $f_c$  between the velocity function for the cosmology of Kravtsov et al. (2004a) (listed above) and the best fit of Tegmark et al. (2006) (the only differences are that in the latter  $\sigma_8 = 0.76$  and  $\Omega_b h^2 = 0.022$ ). Figure 6 shows this ratio as a function of maximum circular velocity. Over the range we will use here, this correction is never more than about 10%. In order to compare our results from the Kravtsov et al. (2004a) simulations to observations, we first apply this correction factor to the predictions from the simulations.

In addition, we have incorporated a “warm dark matter” version of the Tegmark et al. (2006) cosmology that is identical in its large-scale structure, but includes a light dark matter particle, with  $m_{DM} = 0.5$  keV. The lightness of this particle increases its free streaming length, which smooths fluctuations on small scales. Here we apply the adjustment required to the transfer function as outlined by Abazajian (2006). We simply input this new transfer function into the excursion set calculation of the mass function. Of course, on the scales comparable to the free-streaming length, the collapse of structure will cease to be hierarchical, as described by Bode et al. (2001). Thus, almost by definition this prediction will be incorrect; however, we use it as a rough approximation to a more correct prediction which might be available in the future. Figure 6 shows the “correction” as a function of  $V_{\max}$  as the dashed line. In order to predict the warm dark matter case, we apply this correction factor to the simulations.

Figure 7 shows the resulting  $V_{\max}$  functions in the cold dark matter and warm dark matter cases. In the next section, we describe how we compare these theoretical predictions to the observations.

## 5. Comparing theory to observations

The simplest possible comparison we can make between simulations and the observations is to try to put some observed points on the velocity function. After all, we have measured the number density of galaxies as a function of luminosity, and from the Tully-Fisher measurements, we know the relationship between luminosity and the circular velocities. Given the luminosity function of Figure 2 (using the tracers with  $M_r - 5 \log_{10} h < -19$ ), plus the relationship between luminosity and  $V_{\max}$  from Figure 4, we also plot the

observed number density as a function of  $V_{\max}$  as the four points. In this comparison, there appear to be slight discrepancies between the cold dark matter model and the observations, particular at the bright end. The warm dark matter model is nearly as good a fit to the data but somewhat underpredicts (at a bit more than  $1\sigma$ ) the number of isolated low circular velocity galaxies.

However, this method of comparison is sensitive to bias related to scatter in the relationship between luminosity and circular velocity. A more robust comparison can be achieved as follows. For a given predicted circular velocity function and a given observed luminosity function, we can find the relationship between circular velocity and luminosity that makes them consistent with one another. We do so here by parameterizing it as a piecewise linear relationship  $M_r(V_{\max})$  between the circular velocity and a mean absolute magnitude, with Gaussian scatter about that mean. We vary the parameters of the piecewise linear relationship to fit the luminosity function (using the Levenberg-Marquardt method implemented in the IDL routine `mpfit` distributed by Craig B. Markwardt). However, we fix the Gaussian scatter to have  $\sigma_M = 2.5$  for  $V_{\max} \leq 10 \text{ km s}^{-1}$ , to have  $\sigma_M = 0.4$  for  $V_{\max} \geq 100 \text{ km s}^{-1}$ , and to vary linearly with circular velocity in between.

Figure 8 shows the conditional distribution of  $V_{\max}$  as a function of  $M_r$ , given our best fit relationship (using tracers in the simulation with  $V_{\max} > 155 \text{ km s}^{-1}$  and corresponding tracers in the observations with  $M_r - 5 \log_{10} h < -19$ ). The lines are the quartiles of the distribution. The overplotted points are the data from Figure 4. Clearly the median values (shown as the boxes) agree rather well with the predictions. This constitutes a confirmation that the Tully-Fisher relationship and the luminosity function together are consistent with cold dark matter predictions.

How well can these data exclude alternate scenarios? We explore this question by considering the warm dark matter model described above, with a dark matter particle mass of 0.5 keV. We perform the same procedure as described above and obtain the predictions shown in Figure 9. Here, the observed circular velocities of low mass galaxies tend to be higher than predicted, but not by significant amounts. The median is about  $4\sigma$  away from the predicted median, which given the systematic uncertainties here we regard as a marginal exclusion of this model.

## 6. Robustness relative to our definition of “isolated”

Here we examine the robustness of our results to our definition of “isolation,” and how we relate isolation in the observations to isolation in the simulations. There are a number of arbitrary decisions we have made here to define “isolated” in the observations. In particular, we chose a certain projected distance  $r_P$  from galaxies of a certain absolute magnitude  $M_{r,\text{bright}}$  (or brighter). We must examine the sensitivity of our results to these arbitrary choices. In addition, we have also had to define “isolated” in the theoretical predictions. To do so, we have had to relate the absolute magnitude  $M_r$  used above to a  $V_{\max}$  of the halos in the simulation. Of course, we do not know the exact correspondence, and so we need to examine how our results depend on errors in our estimate of it.

Figure 10 examines the sensitivity of our results to both sets of decisions. The top panels show the ratio of the predicted  $\Phi_{\text{iso}}(> V_{\max})$  at  $V_{\max} = 56 \text{ km s}^{-1}$ , to the observed  $\Phi_{\text{iso}}(< M_r)$  at  $M_r - 5 \log_{10} h = -14.7$ . The bottom panels show another comparison of the observations to the theory: the ratio of the observed  $V_{\max} = 56 \text{ km s}^{-1}$  at  $M_r - 5 \log_{10} h = -14.7$  to that predicted by equating the number density of halos larger than a given  $V_{\max}$  to the number density of galaxies brighter than  $M_r - 5 \log_{10} h = -14.7$ . The left panels correspond to our cold dark matter model, and the right panels correspond to our warm dark matter model with  $m_{DM} = 0.5 \text{ keV}$ .

There are 27 points shown on each plot, each corresponding to a different definition of “isolated” in the observations and the theory. First, we check three different choices of tracer sample ( $M_{r,\text{bright}} - 5 \log_{10} h = -18, -19$ , and  $-20$ ), as shown by the rough horizontal position. Second, for each of these three choices of galaxy sample, we choose three different  $V_{\text{max}}$  values with which to define our halo sample for comparison. Our choices of predicted circular velocities for each observed sample are listed in Table 1. In Figure 10, the larger symbols correspond to higher circular velocities. Third, for each of those nine choices, we choose three different choices of  $r_P$  ( $0.7, 1.0$ , and  $1.3 h^{-1}$  Mpc), using the same radius for theory and observation. These three cases are offset from each other slightly in Figure 10 (left to right, respectively) for clarity.

From these results, it is clear that our systematic uncertainties are (fractionally) about 0.3 in the comparison of number densities, and 0.1 in the comparison of circular velocities. The difference is at least partly due to the approximate dependence  $\Phi(> V_{\text{max}}) \propto V_{\text{max}}^{-2.7}$ . In addition, we expect the comparison of circular velocities to be more robust, since it depends less on the scatter in the relationship between luminosity and circular velocity. While for our sample, these systematics are about equivalent to the systematics associated with our surface brightness completeness selection, the systematics shown in Figure 10 illustrate what will ultimately be the most difficult uncertainty to overcome, even when much more complete galaxy samples are available.

## 7. Baryonic and stellar content of low mass galaxies

In the previous section, we showed that the cold dark matter model reasonably explains the number densities and circular velocities of low luminosity galaxies. Assuming that the relationship between circular velocity and total mass that cold dark matter theory predicts is correct, we can now investigate the baryonic and stellar mass content (relative to the total mass) of these low mass galaxies. This census of the matter in dwarf galaxies may help us understand their creation and development over time.

To infer the total mass from  $V_{\text{max}}$  we use the methods of Bullock et al. (2001b), using  $M_* = 1.5 \times 10^{12} h^{-1} M_\odot$  and  $\Omega_m = 0.24$ . These methods have been calibrated down to masses of  $10^{11} h^{-1} M_\odot$ , or about  $85 \text{ km s}^{-1}$ , so our use of them for the lowest luminosity galaxies represents an extrapolation of the current theoretical understanding. At our typical  $V_{\text{max}} \sim 56 \text{ km s}^{-1}$ , the virial mass of the halo determined by this method is  $2.5 \times 10^{10} h^{-1} M_\odot$ .

To infer the stellar mass, we use the optical broadband SDSS data and the methods of Blanton & Roweis (2007). Any method for inferring the total stellar mass is sensitive to the initial mass function (IMF) of stars, since the lowest mass stars (most of those below  $0.5 M_\odot$ ) contribute almost no optical light but are a significant fraction of the mass. The differences between different reasonable choices of IMF can be up to 50%. Blanton & Roweis (2007) have chosen the Chabrier (2003) IMF, and find stellar masses within about 30% of those found for the same galaxies by Kauffmann et al. (2003), using spectroscopic techniques. The median stellar mass for our isolated dwarf galaxy sample is  $2.2 \times 10^7 h^{-2} M_\odot$ .

By “baryonic mass,” we mean here the sum of the stellar mass and neutral gas content, which we take to be  $M_b = M_* + 1.4M_{\text{HI}}$ , where  $M_{\text{HI}}$  is the neutral hydrogen mass inferred from 21cm observations and the factor 1.4 accounts for helium, molecular clouds and metals. The median baryonic mass so defined is  $2.5 \times 10^8 h^{-2} M_\odot$  — much larger than the stellar mass contribution. Naturally, there may also be ionized hydrogen in the galaxy, which we do not try to account for here. Note for the data from Geha et al. (2006a) we do not try to correct for self-absorption of HI, because little evidence for any inclination dependence of the HI to stellar mass ratio is found in our sample. However, Springob et al. (2005) did make such corrections,

which can be up to 20%.

For the samples of isolated galaxies used in this paper, Figure 11 shows the ratio of baryonic mass to total mass as a function of  $r$ -band absolute magnitude (for  $h = 0.7$ ). The dashed line is the cosmic mean based on the results of Tegmark et al. (2006) ( $\Omega_b/\Omega_m = 0.17$ ) and the dotted line is the mean for the sample of Springob et al. (2005) taken alone. The mean of the low luminosity galaxies from Geha et al. (2006a) is somewhat less than that of higher luminosity galaxies, about 8% of the cosmic value rather than 14%. The difference in the treatment of self-absorption may account for about half of this difference.

The baryonic fraction may continue to decrease at lower masses. However, at  $V_{\max} \sim 50 \text{ km s}^{-1}$  isolated low luminosity galaxies do not show much evidence that they have expelled or ionized very much more of their cold gas than have their more massive counterparts. This measurement supports detailed models of the physics of gas blow-out and blow-way due to supernovae, which predict a loss of only a few percent for galaxies in this mass range (Mac Low & Ferrara 1999; Ferrara & Tolstoy 2000; Stinson et al. 2007). However, it disfavors models that prevent star-formation in low mass galaxies through significant baryonic mass loss (Dekel & Silk 1986; Cole et al. 2000; Mori & Burkert 2000; Bullock et al. 2000; Benson et al. 2003; Dekel & Woo 2003; Tremonti et al. 2004; Croton et al. 2006). Of course, reasonable modifications to those models in which feedback prevents the gas from forming stars but keeps it mostly in neutral form and within the galaxy disk are probably tenable. Furthermore, although some investigators have invoked outflows to explain the mass-metallicity relationship, Dalcanton (2007) have shown that alternate models without significant outflow can explain the observations.

We can also look at the relationship between the stellar mass of the galaxies and their total mass. Figure 12 shows the dynamical to stellar mass ratio as a function of stellar mass for the three samples used here. This relationship shows a strong trend, illustrating the strong dependence of star-formation efficiency on mass, at least for disk galaxies. It is, of course, exactly this dependence that causes the luminosity and stellar mass functions to be shallow while the total mass function of galaxies is so steep, as described in Section 1.

## 8. Future directions

The analysis of this paper, while consistent with the CDM model, puts only mild constraints on alternative models (for example, a warm dark matter particle as light as 0.5 keV is barely ruled out). How can this analysis be improved in the future? Two paths are possible: first, increasing the depth and completeness of our optical plus HI sample; second, using upcoming blind HI surveys to push to considerably lower masses. Both paths require improving our understanding of the theoretical predictions at the low mass end.

Our analysis of the current SDSS sample would be substantially improved with more HI follow-up observations. Because Geha et al. (2006a) were studying the general HI properties of dwarfs, we only targeted about 12 systems edge-on enough and isolated enough to include in the analysis of this paper. Our results could be put on a much firmer footing with an increase in our follow up sample. In DR4 there are 64 galaxies with  $b/a < 0.5$ ,  $M_r - 5 \log_{10} h > -15$  and  $r_P > 1 \text{ h}^{-1} \text{ Mpc}$ , and obviously there are still more in later releases. Additional follow-up or deeper HI sky surveys should fill this gap in the future.

The optical SDSS sample on which our analysis here is based will increase by DR8, the final SDSS release, perhaps by a factor of two. However, this will not substantially reduce the uncertainties in the luminosity function, which are already dominated by the surface brightness completeness correction (Figure

1). Blanton et al. (2005) concluded, based on introducing simulated galaxies into raw SDSS imaging data, that the SDSS photometric pipeline (optimized for reasonably high surface brightness galaxies around  $z \sim 0.1$ ) was probably failing at a brighter surface brightness limit than the data required, and that with a differently optimized pipeline it might be possible to push the surface brightness limits to 25 mag or more. Doing so would allow us to probe magnitudes as faint as  $M_r - 5 \log_{10} h \sim -12$  over cosmological volumes. Another possibility would be to wait for upcoming, deeper surveys such as the Dark Energy Survey (DES; Wester et al. 2005), which has first light in late 2010, Pan-STARRS 4 (Hodapp et al. 2004), whose prototype telescope PS1 will probably see first light in 2007, or the Large Scale Synoptic Telescope, which has first light in 2014. Searches for low surface brightness galaxies (through their diffuse light) tend to be dominated by the scattered light background, so it is difficult to anticipate how well of any of these surveys can do. Any of these possibilities would require spectroscopic follow-up — probably searching for 21cm emission in the radio or targeting HII regions in the galaxies.

Blind searches for galaxies in 21cm may show even more promise, particularly since isolated dwarf galaxies virtually always exhibit HI (Geha et al. 2006a) and since the dynamics of each galaxy will be measured simultaneously with its detection. Unfortunately, HIPASS appears to not be deep enough to provide a competitive sample in this respect (many of the SDSS galaxies in our sample are undetectable in HIPASS; Geha et al. 2006a). ALFALFA (Giovanelli et al. 2005) can detect galaxies with HI masses of  $10^7 h^{-2} M_\odot$  at distances of  $20 h^{-1}$  Mpc. If the full 7000 deg<sup>2</sup> planned survey is completed, the overall volume mapped will be about  $6 \times 10^3 h^3$  Mpc<sup>-3</sup>. That large a volume has an expected cosmic variance of around 30%, though given our restriction to isolated regions the actual cosmic variance uncertainties will be lower. Assuming a baryonic to total mass fraction of 0.02 (see Figure 11) and using the methods of Bullock et al. (2001a), this mass corresponds to  $V_{\max} \sim 20$  km s<sup>-1</sup>. Galaxies of this mass in the preliminary ALFALFA catalog of Giovanelli et al. (2007) have a median  $W_{50}$  measurement of  $\sim 40$  km s<sup>-1</sup>, consistent with this estimate. Assuming (conservatively) that 30% cosmic variance errors dominate the uncertainties, using our techniques here one could marginally exclude a warm dark matter particle of 2 keV in mass. Future surveys such as MIRANDA will contribute a similar volume (of a distinct chunk of the Universe), and increase this precision somewhat. In any case, these new HI surveys will push this technique into a low circular velocity regime that is currently only tested with observations of Local Group satellites.

Even to make use of the current data, however, we probably require a better understanding of the theoretical predictions. For example, as we noted above, the excursion set predictions we are making for “warm dark matter” are not entirely self-consistent, since we expect in this regime that the hierarchical picture will start to break down. Under these conditions, Bode et al. (2001) found that the number of forming halos was much smaller than the excursion set prediction. Thus, it may be that our observations would put stronger constraints on a correctly calculated prediction. However, doing so is difficult, since the effective mass resolution for warm dark matter simulations appears to scale much less favorably than for cold dark matter (see Wang & White 2007, who indeed argue that even the number of halos predicted by Bode et al. 2001 is an overestimate).

Finally, it is worth noting two possible *fundamental* limits to the technique we describe here. First, we rely on the 21cm emission to probe the dynamics in the flat part of the rotation curve. While this appears to be the case for most of our galaxies here (based on their double-peaked morphology), it will not necessarily be true of the typical very low mass galaxy. If so, one would need to resort to comparing to cold dark matter predictions in the very inner parts of halos. Second, at lower masses, it may happen that reionization evaporates the lowest mass halos, preventing the formation of stars and the existence of any neutral gas at all. If so, our counting technique will fail. For the galaxies in the mass range we study here, this appears to

be a weak effect, but it may occur at smaller masses.

## 9. Summary

We demonstrate that the predictions of cold dark matter are consistent with the number density of isolated low circular velocity galaxies ( $V_{\max} \sim 50 \text{ km s}^{-1}$ ), at a precision of about 30% (Figures 7 and 8). Our major systematic uncertainties (which dominate our error budget) are related to our definition of “isolated” and our model of the surface brightness completeness of the SDSS at low luminosities. These results represent a valuable independent check of the small-scale predictions of the cold dark matter model. Our technique avoids many of the systematic uncertainties associated with observations of satellite galaxies in the Local Group, related to the complex physics of ram pressure and tidal stripping. From a statistical point of view, our results are less powerful than the current constraints from the Ly $\alpha$  forest power spectrum (Narayanan et al. 2000; Abazajian 2006; Seljak et al. 2006), and only marginally exclude a dark matter particle with  $m_{DM} \sim 0.5 \text{ keV}$ . With an improved sample, this technique will offer a powerful and unique constraint at small scales.

We also find several secondary results that are relevant to the formation of these dwarf galaxies:

1. At low luminosities, the Tully-Fisher relationship appears to be a function of environment, with dwarf satellite galaxies having lower circular velocities than isolated dwarf galaxies, by up to a factor of two or more. There is circumstantial evidence from the nature of the HI profiles that this effect is due to stripping of the outer gas in satellite galaxies, though other processes may be at work.
2. The baryonic mass fraction of galaxies (counting neutral gas plus stars) appears to be a weak function of luminosity down to  $M_r - 5 \log_{10} h \sim -14$ , decreasing by 40% at most (from about 14% to at minimum about 8% the cosmic mean; Figure 12). This result disfavors models which call for a preferentially large amount of baryonic outflow in dwarf galaxies (due to internal processes such as feedback).
3. The ratio of total to stellar mass is a very strong function of stellar mass, ranging from 50 or so at the highest luminosities to over 1000 at the lowest luminosities.

Taken together with the deficit of neutral gas in dwarf galaxies near luminous neighbors (Geha et al. 2006a), these results suggest that the primary effects that remove gas and end star-formation in dwarf galaxies (with circular velocities of  $50 \text{ km s}^{-1}$  or so) are external interactions with bright neighbors, rather than internal processes such as feedback and outflows.

Increasing our sample of isolated dwarf galaxies with HI follow-up (it is straightforward to increase the current sample by more than a factor of five) would improve the precision of all of these results, which are based on a relatively small sample of isolated galaxies. Upcoming blind HI surveys such as the ALFALFA survey on Arecibo are going to impose better constraints on cosmological models at small scales, as well as better explore the issues of dwarf galaxy formation. They will propel the study of field dwarf galaxies into a low circular velocity and low mass regime previously studied only in the Local Group.

We thank Andrey Kravtsov for sharing his simulation results, and Andreas Berlind for his `haloMF` software. For their interest, encouragement, and good discussions, we thank Ari Maller, David W. Hogg, and Beth Willman. We thank Carl Bignell, Toney Minter, and Karen O’Neil for help with the GBT observations. Partial support for this work was provided by NASA-06-GALEX06-0300 and NSF-AST-0428465. MG

acknowledges support from a Plaskett Research Fellowship at the Herzberg Institute of Astrophysics of the National Research Council of Canada. AAW acknowledges the support of NSF grant 0540567.

Funding for the creation and distribution of the SDSS Archive has been provided by the Alfred P. Sloan Foundation, the Participating Institutions, the National Aeronautics and Space Administration, the National Science Foundation, the U.S. Department of Energy, the Japanese Monbukagakusho, and the Max Planck Society. The SDSS Web site is <http://www.sdss.org/>.

The SDSS is managed by the Astrophysical Research Consortium (ARC) for the Participating Institutions. The Participating Institutions are The University of Chicago, Fermilab, the Institute for Advanced Study, the Japan Participation Group, The Johns Hopkins University, the Korean Scientist Group, Los Alamos National Laboratory, the Max-Planck-Institute for Astronomy (MPIA), the Max-Planck-Institute for Astrophysics (MPA), New Mexico State University, University of Pittsburgh, University of Portsmouth, Princeton University, the United States Naval Observatory, and the University of Washington.

## REFERENCES

Abazajian, K. 2006, Phys. Rev. D, 73, 063513

Adelman-McCarthy, J. K. et al. 2006, ApJS, 162, 38

Bahcall, N. A., Dong, F., Bode, P., Kim, R., Annis, J., McKay, T. A., Hansen, S., Schroeder, J., Gunn, J., Ostriker, J. P., Postman, M., Nichol, R. C., Miller, C., Goto, T., Brinkmann, J., Knapp, G. R., Lamb, D. O., Schneider, D. P., Vogeley, M. S., & York, D. G. 2003, ApJ, 585, 182

Begum, A., Chengalur, J. N., Karachentsev, I. D., Kaisin, S. S., & Sharina, M. E. 2006, MNRAS, 365, 1220

Belokurov, V. et al. 2006, astro-ph/0604355

Benson, A. J., Bower, R. G., Frenk, C. S., Lacey, C. G., Baugh, C. M., & Cole, S. 2003, ApJ, 599, 38

Blanton, M., Cen, R., Ostriker, J. P., & Strauss, M. A. 1999, ApJ, 522, 590

Blanton, M. R., Brinkmann, J., Csabai, I., Doi, M., Eisenstein, D. J., Fukugita, M., Gunn, J. E., Hogg, D. W., & Schlegel, D. J. 2003, AJ, 125, 2348

Blanton, M. R. & Roweis, S. 2007, AJ, 133, 734

Blanton, M. R. et al. 2005, AJ, 129, 2562

Blanton, M. R. et al. 2005, ApJ, 631, 208

Bode, P., Ostriker, J. P., & Turok, N. 2001, ApJ, 556, 93

Bottinelli, L., Gouguenheim, L., Paturel, G., & de Vaucouleurs, G. 1983, A&A, 118, 4

Bullock, J. S., Dekel, A., Kolatt, T. S., Kravtsov, A. V., Klypin, A. A., Porciani, C., & Primack, J. R. 2001a, ApJ, 555, 240

Bullock, J. S. & Johnston, K. V. 2005, ApJ, 635, 931

Bullock, J. S., Kolatt, T. S., Sigad, Y., Somerville, R. S., Kravtsov, A. V., Klypin, A. A., Primack, J. R., & Dekel, A. 2001b, MNRAS, 321, 559

Bullock, J. S., Kravtsov, A. V., & Weinberg, D. H. 2000, *ApJ*, 539, 517

Chabrier, G. 2003, *PASP*, 115, 763

Cole, S., Lacey, C. G., Baugh, C. M., & Frenk, C. S. 2000, *MNRAS*, 319, 168

Colín, P., Klypin, A. A., Kravtsov, A. V., & Khokhlov, A. M. 1999, *ApJ*, 523, 32

Conroy, C., Wechsler, R. H., & Kravtsov, A. V. 2005, ArXiv Astrophysics e-prints

Courteau, S. 1997, *AJ*, 114, 2402

Croton, D. J. et al. 2006, *MNRAS*, 365, 11

Dalcanton, J. J. 2007, *ApJ*, 658, 941

de Vaucouleurs, G., de Vaucouleurs, A., Corwin, H. G., Buta, R. J., Paturel, G., & Fouque, P. 1991, Third Reference Catalogue of Bright Galaxies (Volume 1-3, XII, 2069 pp. 7 figs.. Springer-Verlag Berlin Heidelberg New York)

Dekel, A. & Silk, J. 1986, *ApJ*, 303, 39

Dekel, A. & Woo, J. 2003, *MNRAS*, 344, 1131

Desai, V., Dalcanton, J. J., Mayer, L., Reed, D., Quinn, T., & Governato, F. 2004, *MNRAS*, 351, 265

Eisenstein, D. J. & Hu, W. 1998, *ApJ*, 496, 605

Eke, V. R., Baugh, C. M., Cole, S., Frenk, C. S., & Navarro, J. F. 2006, *MNRAS*, 370, 1147

Faber, S. M. & Jackson, R. E. 1976, *ApJ*, 204, 668

Ferrara, A. & Tolstoy, E. 2000, *MNRAS*, 313, 291

Gao, L., White, S. D. M., Jenkins, A., Stoehr, F., & Springel, V. 2004, *MNRAS*, 355, 819

Geha, M., Blanton, M. R., Masjedi, M., & West, A. A. 2006a, *ApJ*, 653, 240

Geha, M., Guhathakurta, P., Rich, R. M., & Cooper, M. C. 2006b, *AJ*, 131, 332

Giovanelli, R., Haynes, M. P., Kent, B. R., Saintonge, A., Stierwalt, S., Altaf, A., Balonek, T., Brosch, N., Brown, S., Catinella, B., Furniss, A., Goldstein, J., Hoffman, G. L., Koopmann, R. A., Kornreich, D. A., Mahmood, B., Martin, A. M., Masters, K. L., Mitschang, A., Momjian, E., Nair, P. H., Rosenberg, J. L., & Walsh, B. 2007, *AJ*, 133, 2569

Giovanelli, R. et al. 2005, *AJ*, 130, 2598

Goldberg, D. M., Jones, T. D., Hoyle, F., Rojas, R. R., Vogeley, M. S., & Blanton, M. R. 2005, *ApJ*, 621, 643

Hernquist, L. 1993, *ApJS*, 86, 389

Hodapp, K. W., Kaiser, N., Aussel, H., Burgett, W., Chambers, K. C., Chun, M., Dombeck, T., Douglas, A., Hafner, D., Heasley, J., Hoblitt, J., Hude, C., Isani, S., Jedicke, R., Jewitt, D., Laux, U., Luppino, G. A., Lupton, R., Maberry, M., Magnier, E., Mannery, E., Monet, D., Morgan, J., Onaka, P., Price, P., Ryan, A., Siegmund, W., Szapudi, I., Tonry, J., Wainscoat, R., & Waterson, M. 2004, *Astronomische Nachrichten*, 325, 636

Ibata, R. A., Gilmore, G., & Irwin, M. J. 1995, MNRAS, 277, 781

Jenkins, A., Frenk, C. S., White, S. D. M., Colberg, J. M., Cole, S., Evrard, A. E., Couchman, H. M. P., & Yoshida, N. 2001, MNRAS, 321, 372

Karachentsev, I. D., Karachentseva, V. E., Huchtmeier, W. K., & Makarov, D. I. 2004, AJ, 127, 2031

Kauffmann, G. et al. 2003, MNRAS, 341, 33

Klypin, A., Kravtsov, A. V., Valenzuela, O., & Prada, F. 1999, ApJ, 522, 82

Kravtsov, A. V., Berlind, A. A., Wechsler, R. H., Klypin, A. A., Gottlöber, S., Allgood, B., & Primack, J. R. 2004a, ApJ, 609, 35

Kravtsov, A. V., Gnedin, O. Y., & Klypin, A. A. 2004b, ApJ, 609, 482

Mac Low, M.-M. & Ferrara, A. 1999, ApJ, 513, 142

Mateo, M. L. 1998, ARA&A, 36, 435

Mayer, L., Mastropietro, C., Wadsley, J., Stadel, J., & Moore, B. 2006, MNRAS, 369, 1021

Mori, M. & Burkert, A. 2000, ApJ, 538, 559

Narayanan, V. K., Spergel, D. N., Davé, R., & Ma, C.-P. 2000, ApJ, 543, L103

Pizagno, J., Prada, F., Weinberg, D. H., Rix, H.-W., Pogge, R. W., Grebel, E. K., Harbeck, D., Blanton, M., Brinkmann, J., & Gunn, J. E. 2006, AJ, submitted (astro-ph/0608472)

Reed, D., Gardner, J., Quinn, T., Stadel, J., Fardal, M., Lake, G., & Governato, F. 2003, MNRAS, 346, 565

Reed, D., Governato, F., Quinn, T., Gardner, J., Stadel, J., & Lake, G. 2005, MNRAS, 359, 1537

Rees, M. J. & Ostriker, J. P. 1977, MNRAS, 179, 541

Rines, K., Diaferio, A., & Natarajan, P. 2006, ArXiv Astrophysics e-prints

Robertson, B., Bullock, J. S., Font, A. S., Johnston, K. V., & Hernquist, L. 2005, ApJ, 632, 872

Seljak, U., Makarov, A., Mandelbaum, R., Hirata, C. M., Padmanabhan, N., McDonald, P., Blanton, M. R., Tegmark, M., Bahcall, N. A., & Brinkmann, J. 2005, Phys. Rev. D, 71, 043511

Seljak, U., Makarov, A., McDonald, P., & Trac, H. 2006, Phys. Rev. Lett., submitted, (astro-ph/0602430)

Sheth, R. K., Mo, H. J., & Tormen, G. 2001, MNRAS, 323, 1

Simon, J. D. & Geha, M. 2007, ArXiv e-prints, 706

Somerville, R. S., Lemson, G., Sigad, Y., Dekel, A., Kauffmann, G., & White, S. D. M. 2001, MNRAS, 320, 289

Spergel, D. N. et al. 2006, astro-ph/0603449

Springob, C. M., Haynes, M. P., Giovanelli, R., & Kent, B. R. 2005, ApJS, 160, 149

Stinson, G. S., Dalcanton, J. J., Quinn, T., Kaufmann, T., & Wadsley, J. 2007, ArXiv e-prints, 705

Stoehr, F., White, S. D. M., Tormen, G., & Springel, V. 2002, MNRAS, 335, L84

Swaters, R. A., van Albada, T. S., van der Hulst, J. M., & Sancisi, R. 2002, A&A, 390, 829

Tasitsiomi, A., Kravtsov, A. V., Wechsler, R. H., & Primack, J. R. 2004, ApJ, 614, 533

Tegmark, M. et al. 2006, Phys. Rev. D, 74, 123507

Tremonti, C. A. et al. 2004, ApJ, 613, 898

Trentham, N., Sampson, L., & Banerji, M. 2005, MNRAS, 357, 783

Tully, R. B. & Fisher, J. R. 1977, A&A, 54, 661

Wang, J. & White, S. D. M. 2007, ArXiv Astrophysics e-prints

Warren, M. S., Abazajian, K., Holz, D. E., & Teodoro, L. 2006, ApJ, 646, 881

Wester, W. et al. 2005, in Astronomical Society of the Pacific Conference Series, Vol. 339, Observing Dark Energy, ed. S. C. Wolff & T. R. Lauer, 152–+

White, S. D. M. & Frenk, C. S. 1991, ApJ, 379, 52

White, S. D. M. & Rees, M. J. 1978, MNRAS, 183, 341

Willlick, J. A., Strauss, M. A., Dekel, A., & Kolatt, T. 1997, ApJ, 486, 629

Willman, B., Blanton, M. R., West, A. A., Dalcanton, J. J., Hogg, D. W., Schneider, D. P., Wherry, N., Yanny, B., & Brinkmann, J. 2005a, AJ, 129, 2692

Willman, B., Dalcanton, J. J., Martinez-Delgado, D., West, A. A., Blanton, M. R., Hogg, D. W., Barentine, J. C., Brewington, H. J., Harvanek, M., Kleinman, S. J., Krzesinski, J., Long, D., Neilsen, E. H., Nitta, A., & Snedden, S. A. 2005b, ApJ, 626, L85

Yahagi, H., Nagashima, M., & Yoshii, Y. 2004, ApJ, 605, 709

York, D. et al. 2000, AJ, 120, 1579

Zentner, A. R., Berlind, A. A., Bullock, J. S., Kravtsov, A. V., & Wechsler, R. H. 2005, ApJ, 624, 505

Zucker, D. B. et al. 2006a, ArXiv Astrophysics e-prints

Zucker, D. B. et al. 2006b, ApJ, 643, L103

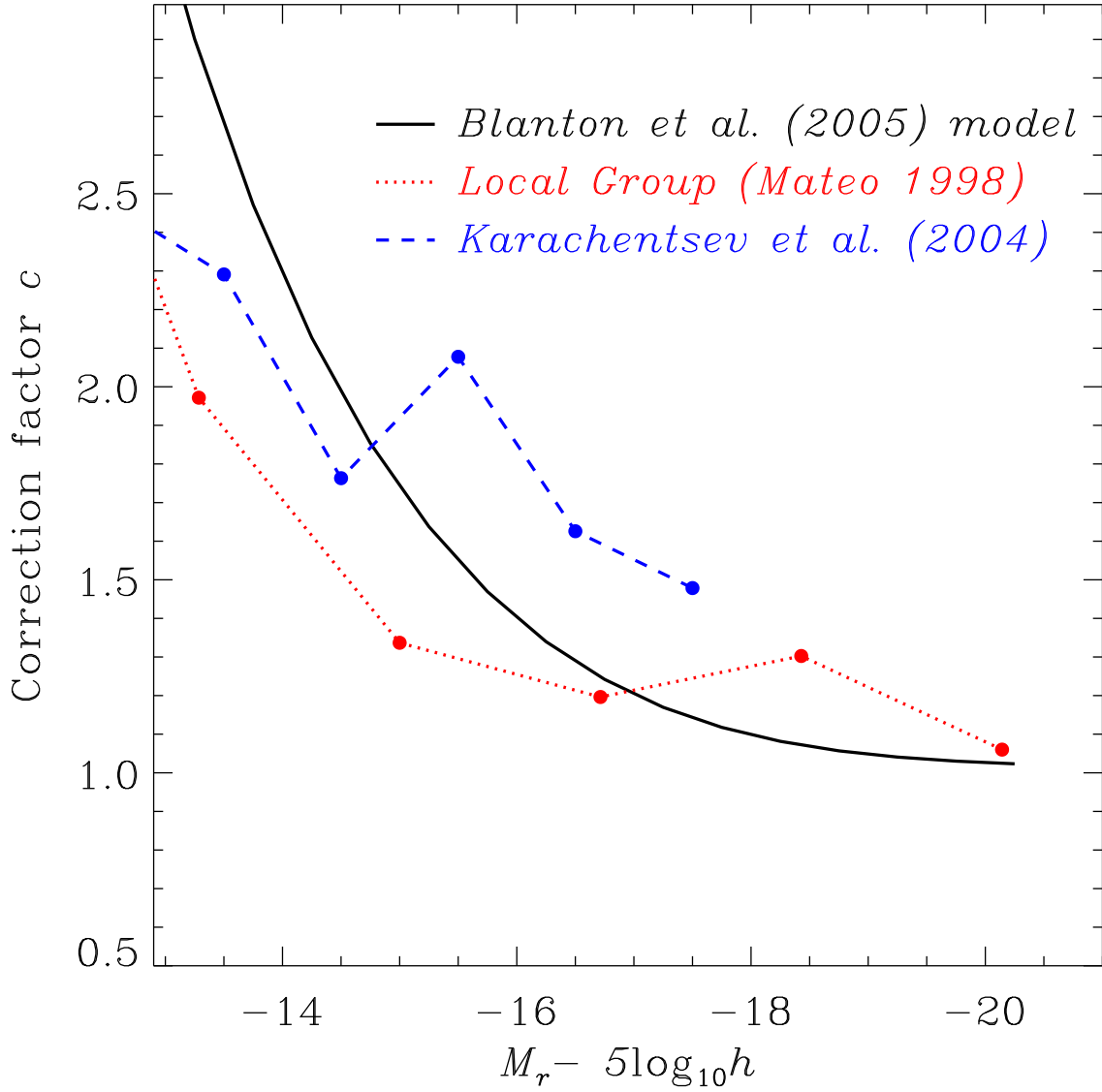


Fig. 1.— Estimates of necessary correction factors  $c$  for surface brightness incompleteness as a function of absolute magnitude. The solid line is the estimate from Blanton et al. (2005) using a simple model of surface brightness as a function of absolute magnitude and determinations of the completeness of SDSS as a function of surface brightness. The dashed line uses the distribution of surface brightnesses as a function of absolute magnitude from the local catalog of Karachentsev et al. (2004). The dotted line uses the distribution from the Local Group according to Mateo (1998).

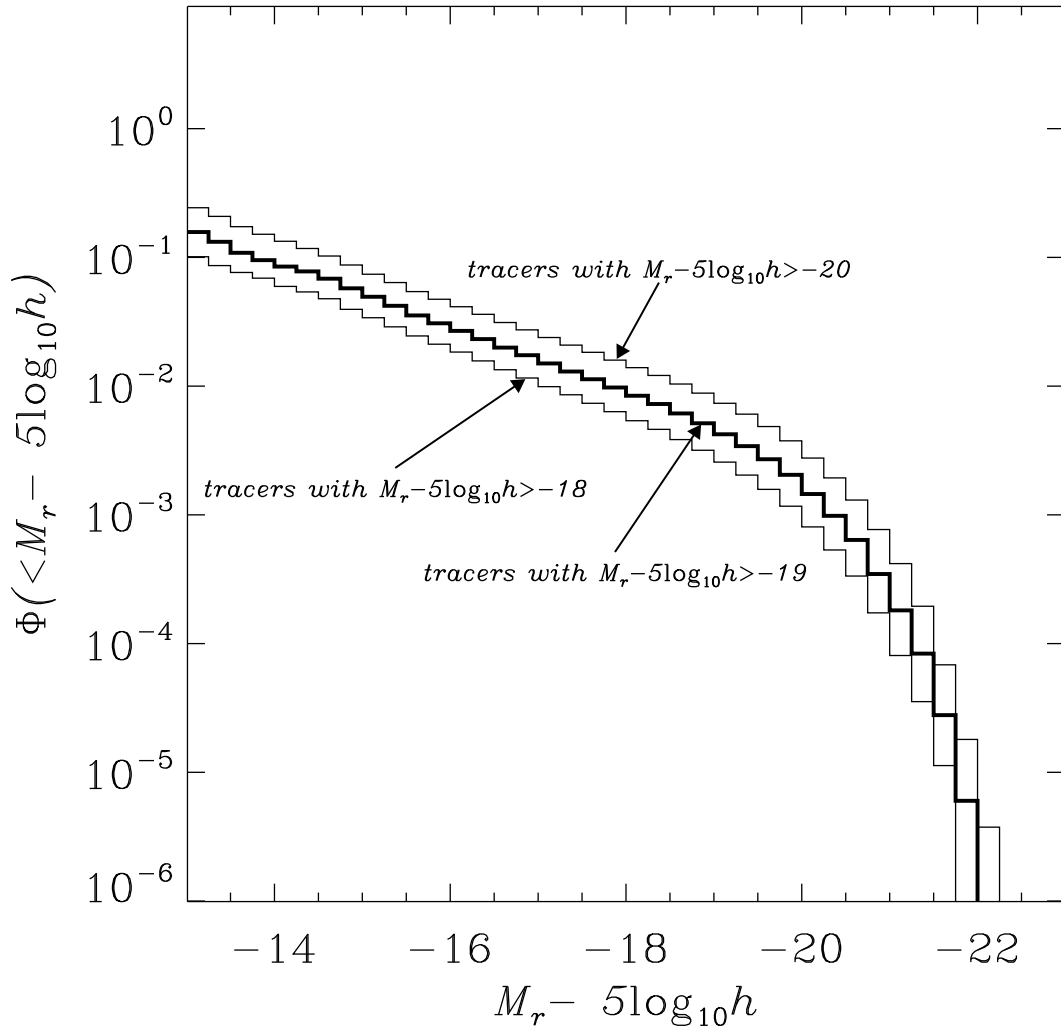


Fig. 2.— Cumulative luminosity function of isolated galaxies, as defined in the text. The meaning of “isolated” depends on the tracer galaxies used. The thick histogram represents the median relationship using tracer galaxies with  $M_r - 5\log_{10} h < -19$ . The thin histogram represents a change of 1 magnitude in the absolute magnitude limit used for the tracer galaxies; the upper histogram uses brighter galaxies, and the lower histogram uses fainter galaxies.

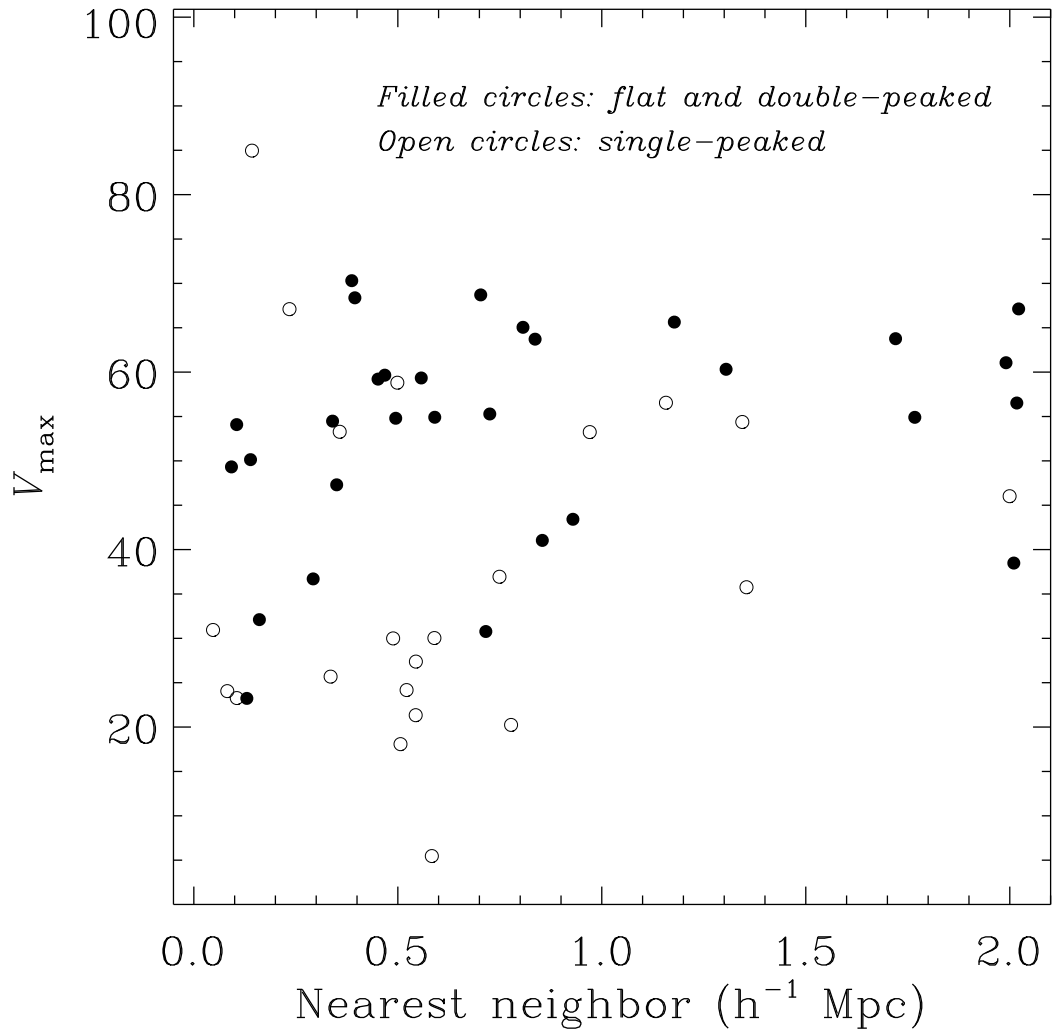


Fig. 3.— Estimate of  $V_{\max}$  for dwarf galaxies in our sample as a function of distance to the nearest luminous neighbor galaxy. Filled symbols are galaxies with flat or double-peaked HI profiles, open symbols are galaxies with single-peaked HI profiles.

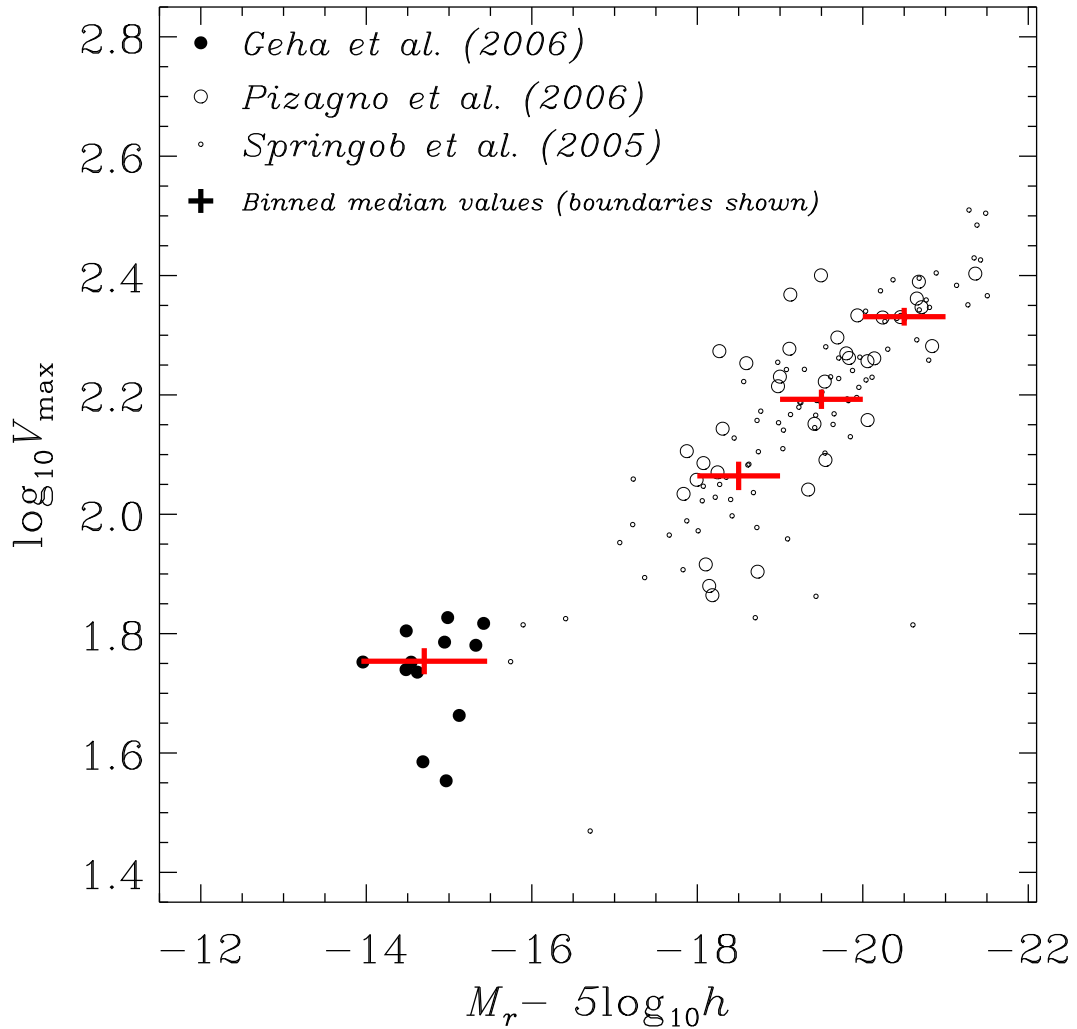


Fig. 4.— Tully-Fisher relation for isolated galaxies. Large open symbols are from the optical rotation curves of Pizagno et al. (2006), small open symbols are from the compilation of Springob et al. (2005), and filled symbols are from the HI linewidths of Geha et al. (2006b). Crosses show the median  $V_{\max}$  values in several bins; the bin centers and median values are listed in Table 1.

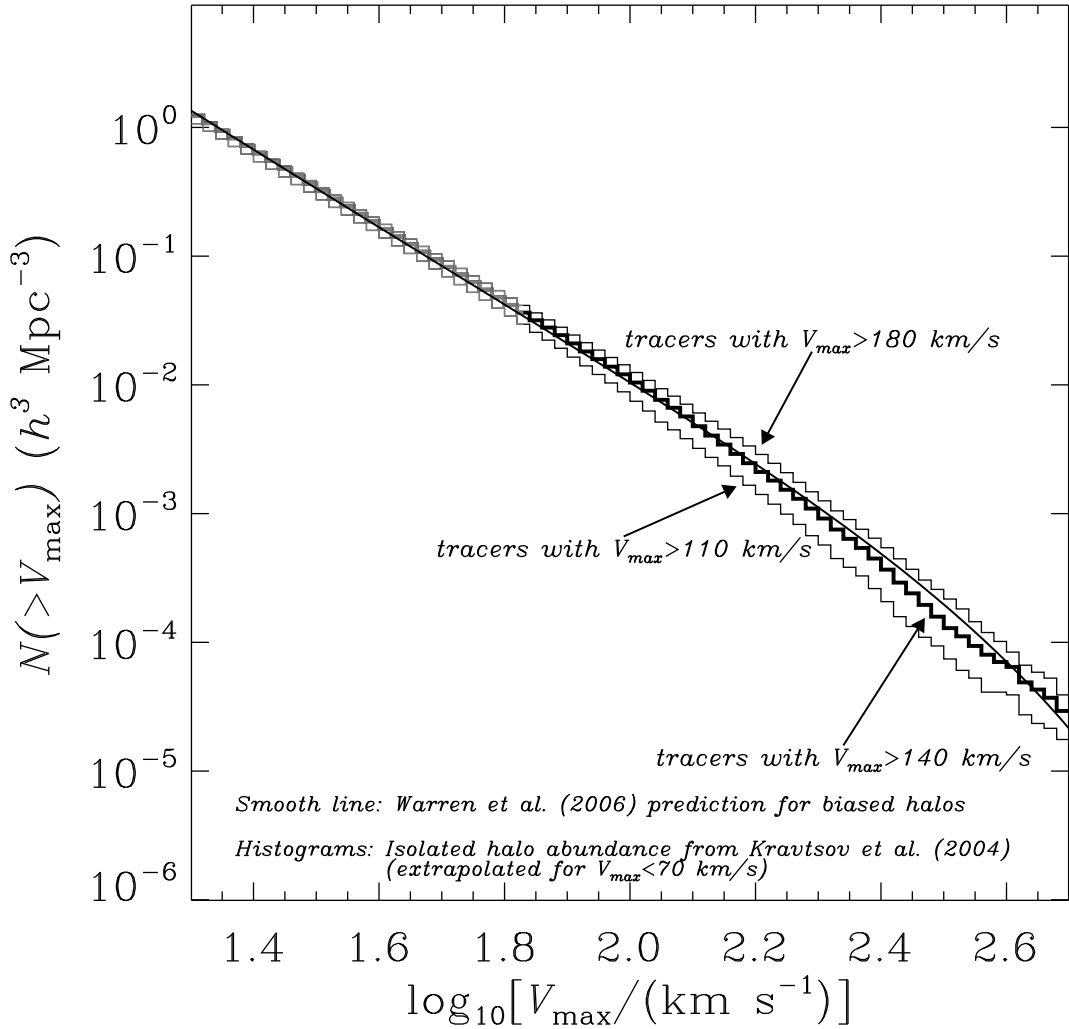


Fig. 5.— Cumulative  $V_{\max}$  function of isolated halos from  $N$ -body simulations, for various choices of tracers. The thick histogram is the abundance of halos in the simulation subject to the isolation criterion described in the text, based on the projected distance and redshift different relative to the nearest, other “tracer” halo, for tracers with  $V_{\max} > 140 \text{ km s}^{-1}$ . The thin histograms explore the effect of trying different tracer populations, as labeled. The smooth line is an approximation based on the mass functions of Warren et al. (2006), described more fully in the text, using a relative large-scale bias of  $\delta = -0.4$  for the halos.

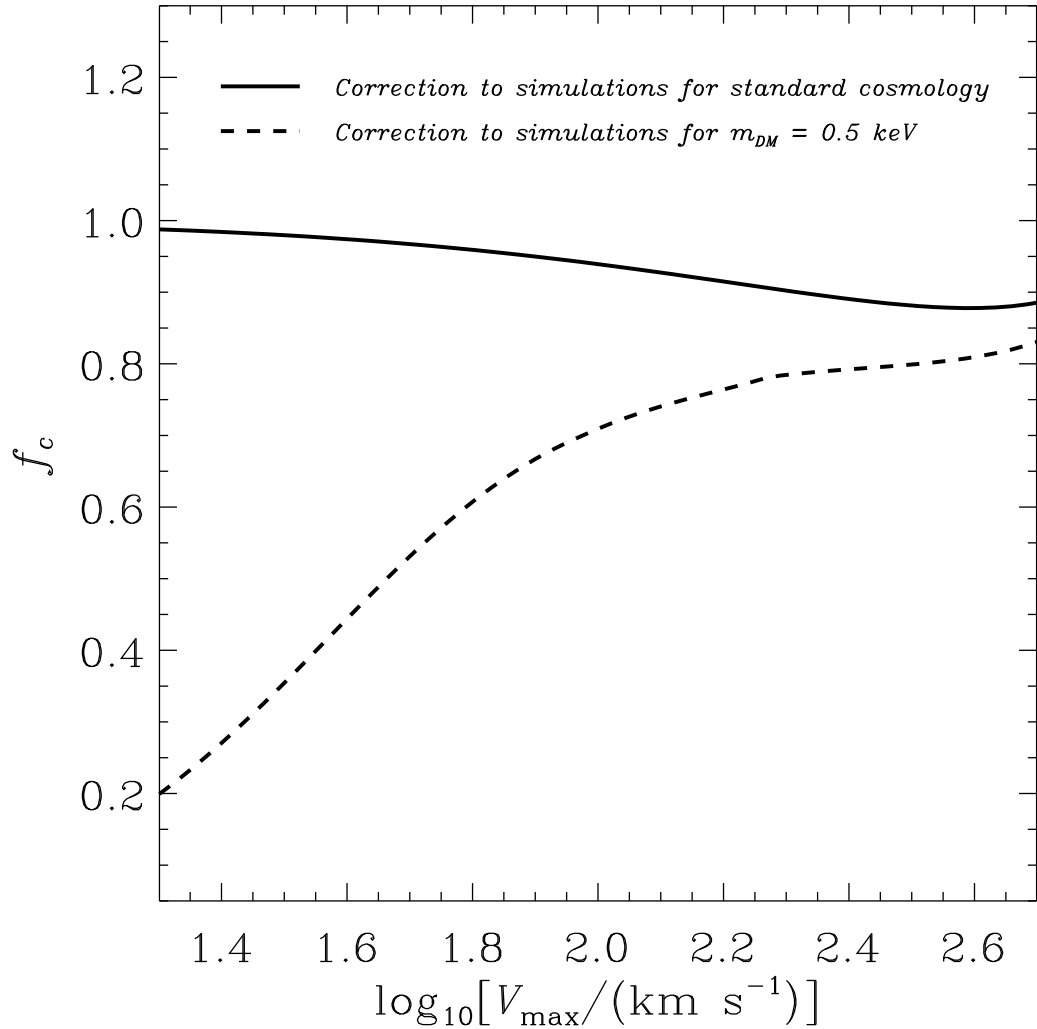


Fig. 6.— Correction to the mass function between the cosmology of the  $N$ -body simulations of Kravtsov et al. (2004a) and the cosmological models we want to test. The solid line is the correction to the standard cosmology of Tegmark et al. (2006) based on WMAP and SDSS large-scale data. The dashed line is the correction to that same cosmology, but with a light dark matter particle ( $m_{\text{DM}} = 0.5 \text{ keV}$ ). Corrections are based on the ratio between the appropriate cosmologies in the approximations of Warren et al. (2006).

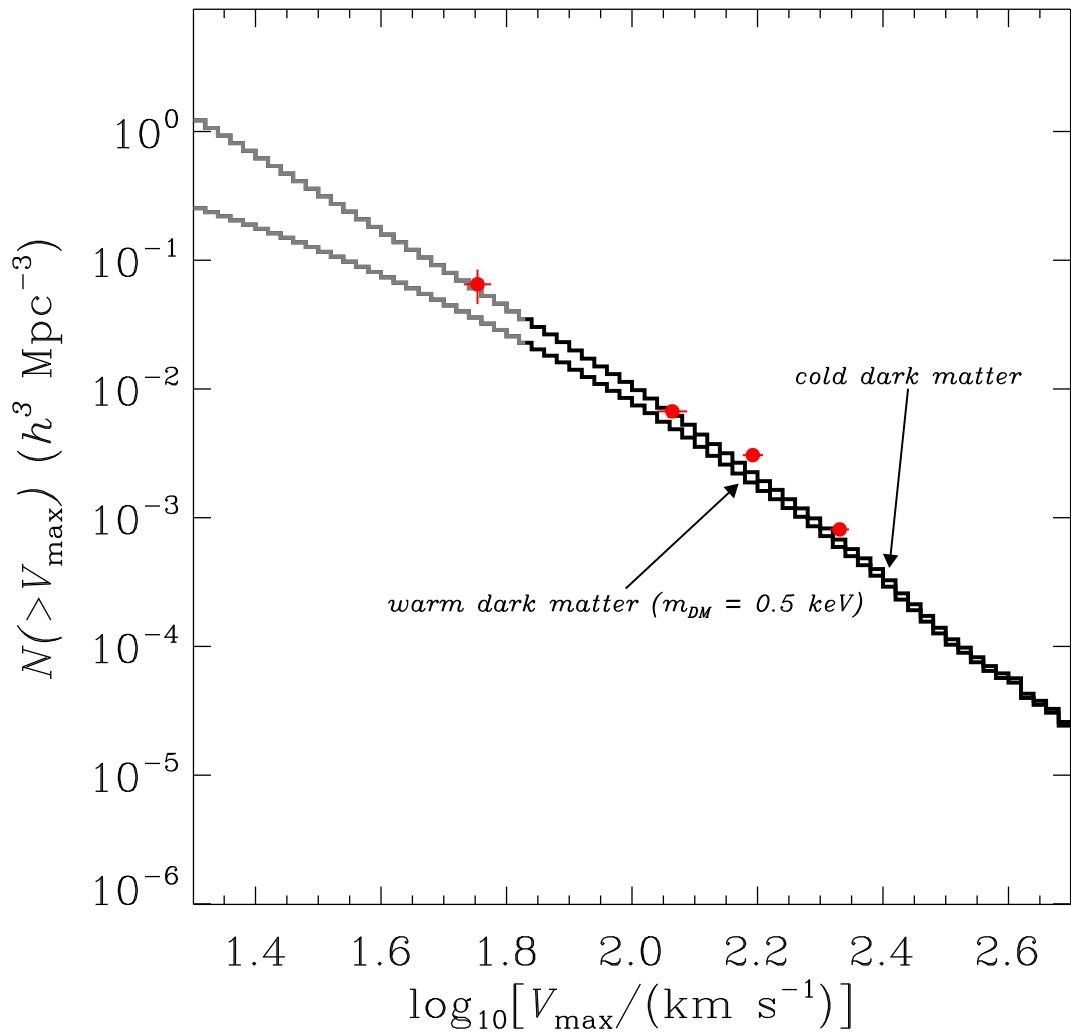


Fig. 7.— Cumulative  $V_{\max}$  function of isolated halos from Figure 5, corrected to the Tegmark et al. (2006) cosmology (upper histogram) and that same cosmology with a light dark matter particle (lower histogram).

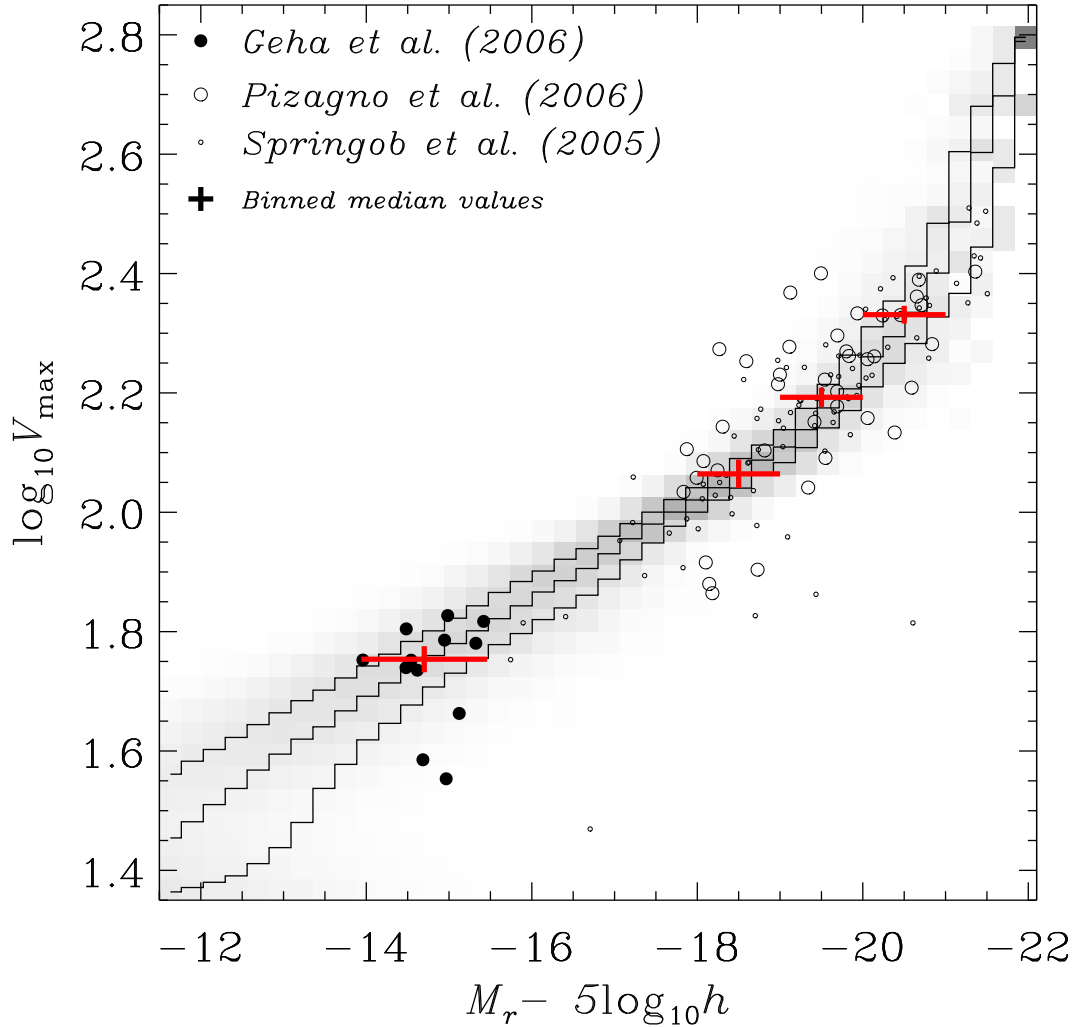


Fig. 8.— Conditional distribution of circular velocity as a function of absolute magnitude, to make our observed isolated galaxy luminosity function consistent with the predicted isolated halo circular velocity function. Lines are the quartiles of the distribution. The overplotted points and binned median values are the data from Figure 4.

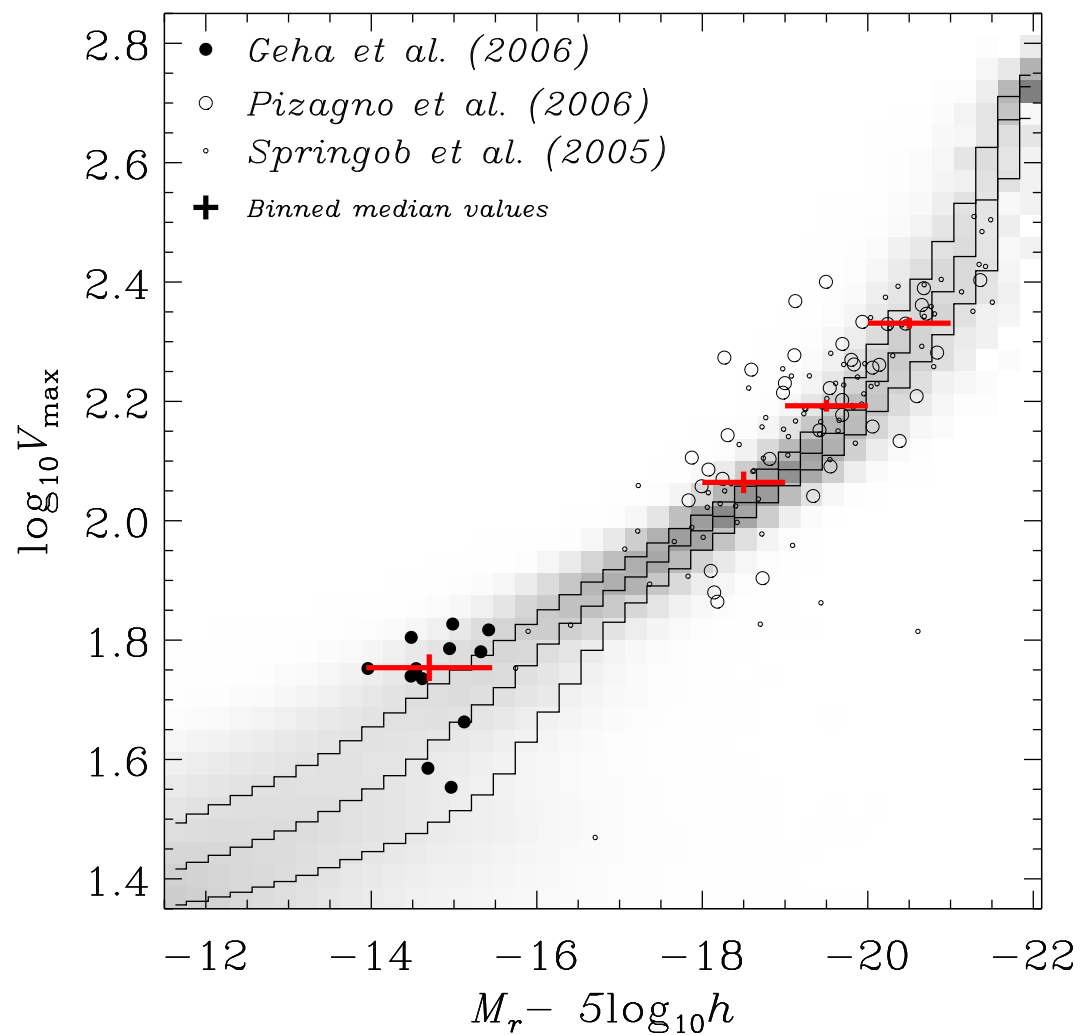


Fig. 9.— Similar to Figure 8 but based on the warm dark matter models.

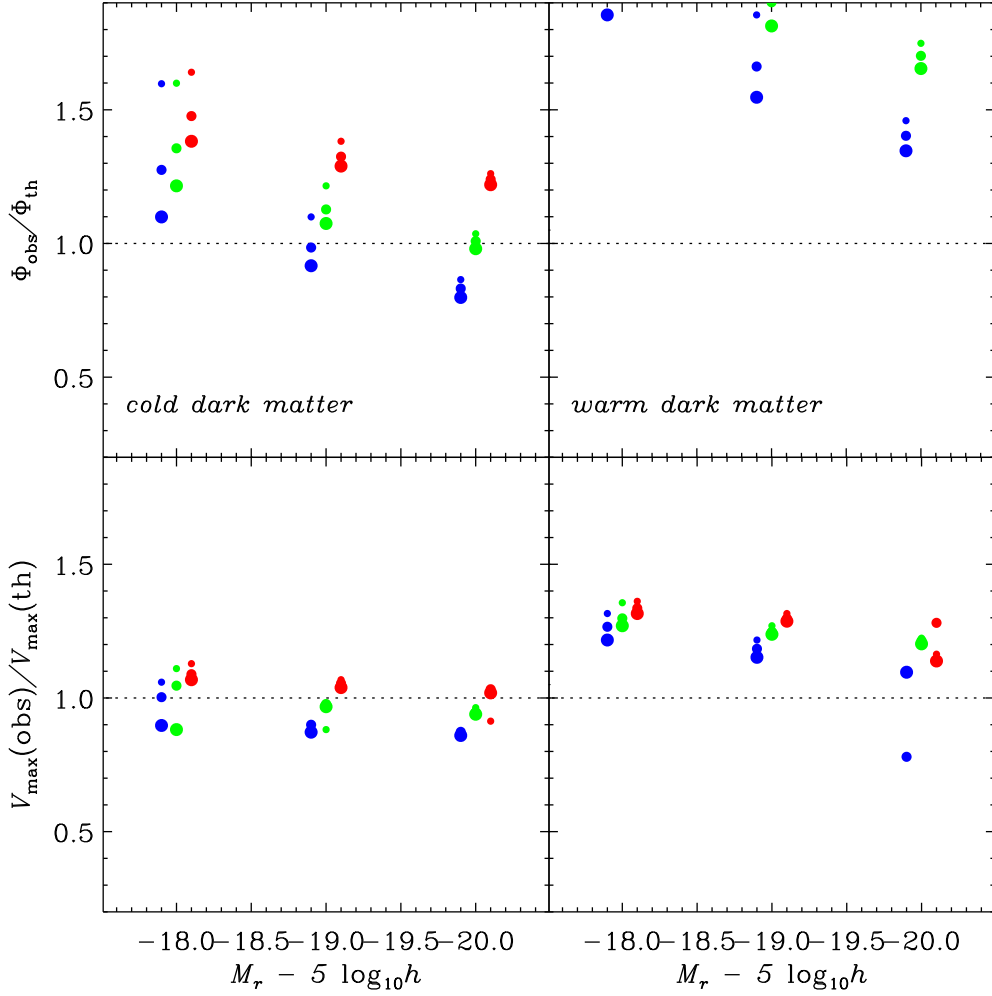


Fig. 10.— Dependence of our results on our definition of “isolated.” The left panels refer to our cold dark matter model. The right panels refer to the warm dark matter model with  $m_{DM} = 0.5$  keV. The top panels show the ratio of the observed number density of isolated galaxies with  $M_r - 5 \log_{10} h < -14.7$  to the predicted number of isolated halos with  $V_{\max} > 56 \text{ km s}^{-1}$  (that is, the vertical offset in Figure 7). The bottom panels show the ratio between the median observed circular velocity at  $M_r - 5 \log_{10} h < -14.7$  to that predicted in Figures 8 and 9. All of these results are shown as a function of how we define “isolated,” which we do in 27 different ways here. We choose: (a) three different absolute magnitude limits for the tracers in the observed sample,  $M_r - 5 \log_{10} h < -18$ ,  $-19$ , and  $-20$ , as shown by the rough horizontal position; (b) for each sort of observed tracer, three choices of minimum  $V_{\max}$  for tracers in the predicted sample, as listed in Table 1 and as shown by the size of the symbols (larger corresponds to higher circular velocity of tracer); and (c) three different minimum projected radii from the tracers,  $r_P = 0.7$ ,  $1.0$ , and  $1.3 h^{-1} \text{ Mpc}$ , as shown by small offsets in the horizontal positions (left to right).

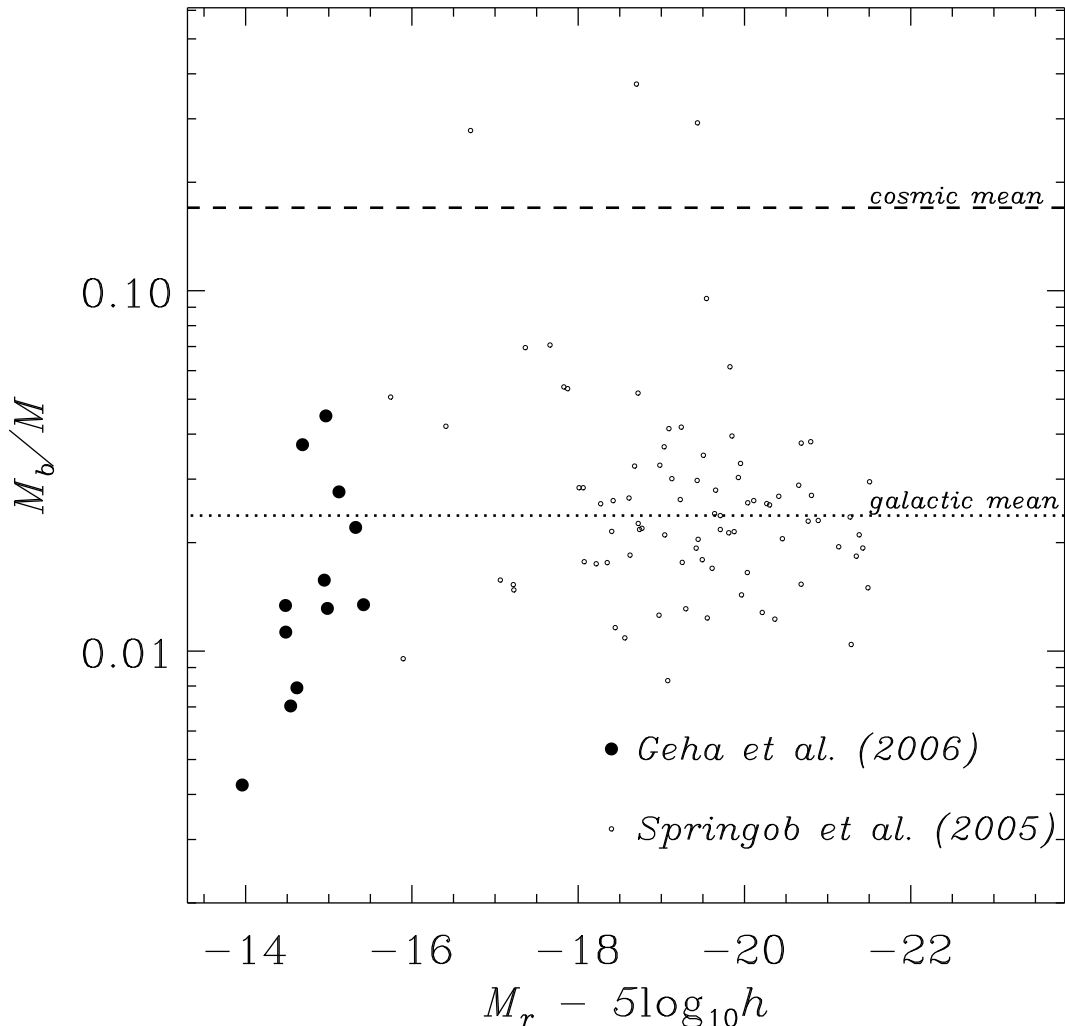


Fig. 11.— “Baryonic” mass relative to total mass as a function of luminosity for the samples of isolated galaxies with  $b/a < 0.5$  in the two HI samples used here, as marked. Baryonic mass is defined as the stellar mass plus the neutral gas mass, as described in the text. The dashed line at 0.17 is the cosmic mean based on cosmological measurements (Tegmark et al. 2006). The dotted line at 0.025 is the mean of the Springob et al. (2005) measurements.

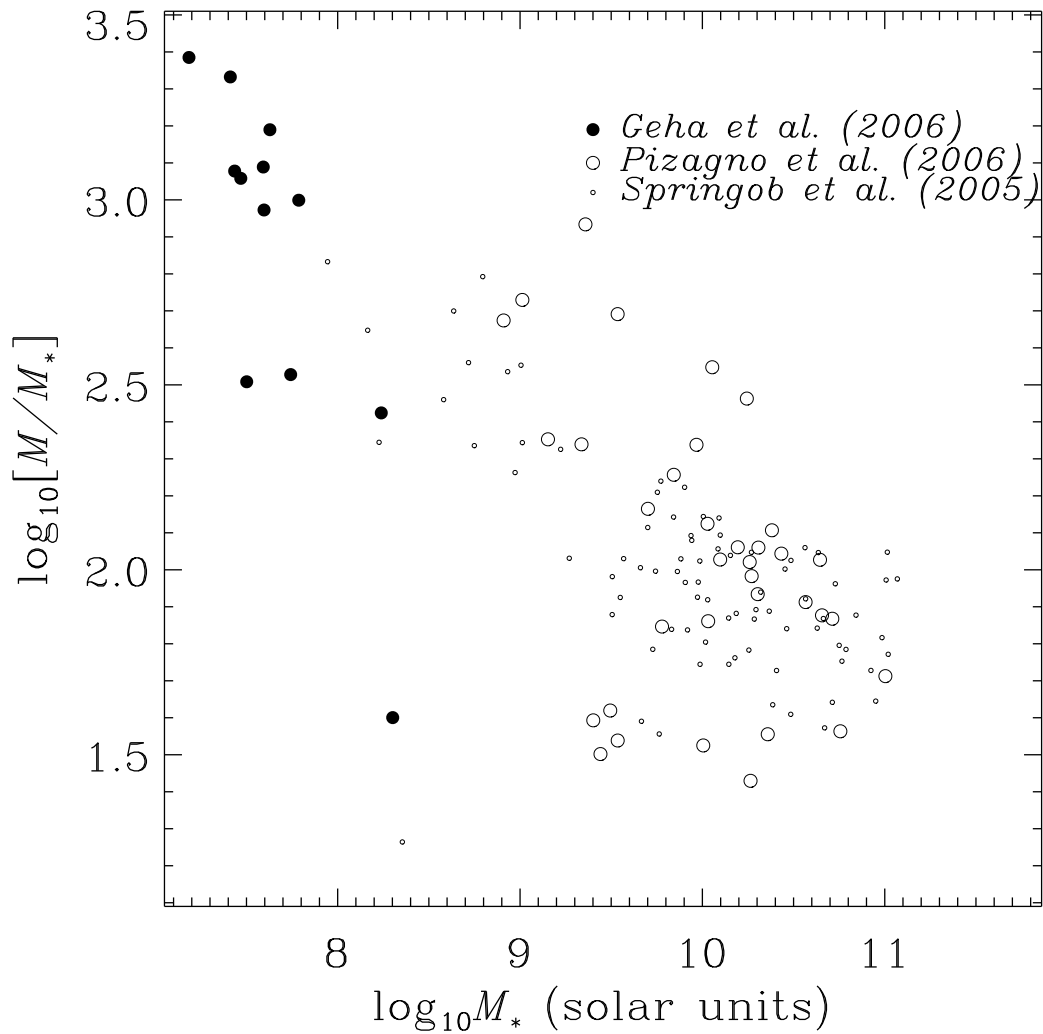


Fig. 12.— Dynamical to stellar mass ratio as a function of stellar mass, for the three samples used in this paper (restricting to isolated galaxies with  $b/a < 0.5$ ).

Table 1. Comparable circular velocities and absolute magnitudes

$M_r - 5 \log_{10} h$	$V_{\max}$ (km s $^{-1}$ )	$V_{\max}$ (km s $^{-1}$ )
	(from TF)	(used)
–14.7	56 ± 3	—
–18.0	108 ± 5	95, 110, 125
–18.5	116 ± 6	—
–19.0	143 ± 7	125, 140, 155
–19.5	156 ± 7	—
–20.0	180 ± 4	170, 180, 195
–20.5	214 ± 7	—

Note. — For each choice of  $M_r$  (first column), this table yields the comparable  $V_{\max}$  resulting from matching to the Tully-Fisher relation in Figure 4 (second column, “TF”). It also lists the  $V_{\max}$  values we actually tried in Figure 10 (third column).